

Signatures of quantum chaos in rare-earth elements: I. Characterization of the Hamiltonian matrices and coupling matrices of Ce I and Pr I using the statistical predictions of Random Matrix Theory

To cite this article: A Cummings *et al* 2001 *J. Phys. B: At. Mol. Opt. Phys.* **34** 3407

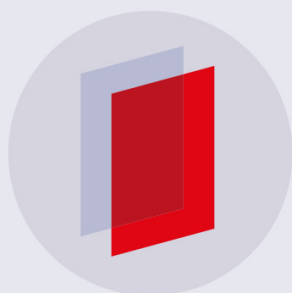
View the [article online](#) for updates and enhancements.

Related content

- [Signatures of quantum chaos in rare earth elements:II](#)
A Cummings, G O'Sullivan and D M Heffernan
- [Characterization of the structure and eigenvalue spectra of the compound states of Sm IX](#)
D Kilbane, A Cummings, D M Heffernan *et al.*
- [B-splines in atomic and molecular physics](#)
H Bachau, E Cormier, P Decleva *et al.*

Recent citations

- [Many-body quantum chaos: Recent developments and applications to nuclei](#)
J.M.G. Gómez *et al*
- [Random matrix structure of nuclear shell model Hamiltonian matrices and comparison with an atomic example](#)
Manan Vyas and V. K. B. Kota
- [Characterization of the structure and eigenvalue spectra of the compound states of Sm IX](#)
D Kilbane *et al*



IOP | ebooks™

Bringing you innovative digital publishing with leading voices to create your essential collection of books in STEM research.

Start exploring the collection - download the first chapter of every title for free.

Signatures of quantum chaos in rare-earth elements: I. Characterization of the Hamiltonian matrices and coupling matrices of Ce I and Pr I using the statistical predictions of Random Matrix Theory

A Cummings^{1,2}, G O'Sullivan¹ and D M Heffernan^{2,3}

¹ Physics Department, University College Dublin, Dublin 4, Ireland

² Department of Mathematical Physics, National University of Ireland Maynooth, Maynooth, Co. Kildare, Ireland

³ School of Theoretical Physics, Dublin Institute for Advanced Studies, Dublin 4, Ireland

Received 5 April 2001, in final form 15 June 2001

Published 21 August 2001

Online at stacks.iop.org/JPhysB/34/3407

Abstract

Using the relativistic configuration interaction Hartree–Fock method the Hamiltonian matrices of Ce I, $J = 4^\pm$, and Pr I, $J = 11/2^\pm$, are studied. These matrices can be characterized as sparse, banded matrices, with a leading diagonal. Diagonalization of the Hamiltonian results in a set of energy eigenvalues and corresponding eigenvectors and the purpose of this investigation will be to characterize the Hamiltonian matrices and coupling matrices of Ce I and Pr I, for both ls and jj coupling representations, using various statistical predictions of Random Matrix Theory.

1. Introduction

Recent studies [1–3] of neutral Ce have claimed that this atom is an example of a many-body quantum chaotic system. If this is so, then it should be expected that the next element along the rare earth sequence, namely Pr, which has five valence electrons ‘moving’ in the field of the core, should also exhibit quantum chaotic signatures. This study will therefore consist of two parts: part I, the purpose of which, using [1–5] as guidelines, will be to examine the Hamiltonian matrices and coupling matrices of both Ce I, $J = 4^\pm$, and Pr I, $J = 11/2^\pm$, and to compare the results with the various statistical predictions of Random Matrix Theory (RMT) [6]; and part II, ‘Characterization of the energy eigenvalues and dipole moments of Ce I and Pr I’, the purpose of which is as described.

It is important to stress that parts I and II will include additional statistical tests that have not been used, to date, in previous studies [1–3] of the lanthanide elements. These include the information entropy/length, moments of the wavefunction $|\text{amplitude}|^2$ and the correlation of eigenvector components. Also, it must be emphasized that in [1] single determinant basis

states were used, which is not the most physically realistic coupling representation. Therefore in part I of this study the effects of the more physically viable ls and jj coupling schemes are investigated. In part II invariant spectral measures will be utilized, namely the spectral rigidity, covariance of adjacent spacings and the correlation-hole method. These invariant statistics are not basis representation dependent and so are a more reliable indicator of quantum chaotic behaviour.

The reason for choosing Ce, $J = 4^\pm$, was to compare the Cowan code (HFCI) [7] results with the Hartree–Fock–Dirac (HFD) calculations used in [1]. The HFD calculations are fully relativistic as compared to the Cowan code, which, although using the configuration interaction approach, uses bases constructed from the independent particle model with an effective mean field. This is inherently non-many-body in its approach, although configuration interactions do partially compensate for this deficit and in doing so introduce correlation effects. The rationale for choosing Pr and $J = 11/2^\pm$ was to compare and contrast its results with those of Ce, the $J = 11/2^\pm$ states having significantly more Hamiltonian matrix elements. Also, additionally, for Pr, the $11/2^\pm$ angular momentum states had the largest number of experimental energy levels available [8].

Prior to the actual diagonalization, one can study important characteristics of the system by analysing the properties of the Hamiltonian matrix.

2. Banded Hamiltonian matrices

Considerable progress has been made in generalizing RMT to banded random matrices (BRMs) [9–11] during the last several years. In contrast to the orthogonal, unitary or symplectic Gaussian ensembles with the distribution functions invariant under transformations preserving the corresponding symmetry, the BRM are given in a ‘special’ basis. In this basis, the basis states are ordered in such a way that a Hamiltonian matrix has a band of non-zero matrix elements H_{ij} interconnecting the states within the band $|i - j| \leq b$ around the main diagonal, i.e. a basis state is coupled to, at most, $2b$ other basis states and to at least b other basis states.

The number b is called the number bandwidth of the band. For the Gaussian distribution of the non-zero matrix elements, the properties of the ensemble are predicted [11] to be determined by the scaling parameter b^2/N , where N is the matrix dimension.

The banded structure of the shell-model Hamiltonian is in fact the reflection of the selection rules specific for the two-body interaction.

The Hamiltonian of a particular atomic system can be approximated by [7]

$$H = \sum_{i=1}^N \left[\frac{p_i^2}{2m} - \frac{Ze^2}{r_i} + \xi(r_i) l_i \cdot s_i \right] + \sum_i \sum_{j>i} \frac{e^2}{r_{ij}}. \quad (1)$$

The configurations of table 1 were used as basis configurations for Ce 1 (as used in the study of [1]) and Pr 1. The even- and odd-parity configurations of both species will henceforth be referred to as ‘even Ce/Pr’ and ‘odd Ce/Pr’ respectively.

In order to show the bandedness of the Hamiltonian matrices the windowed averaged $\langle H^2 \rangle_{ij}$ [1, 2]

$$\langle H^2 \rangle_{ij} = \frac{1}{(2W + 1)^2} \sum_{\substack{|i'-i| \leq W \\ |j'-j| \leq W}} H_{i'j'}^2 \quad (2)$$

were calculated and are shown in figures 1 and 2. W is the size of the averaging ‘window’ used and values of 9 and 18 were chosen for Ce and Pr respectively, i.e. square windows of

Table 1. The even and odd configurations of Ce I and Pr I.

Ce I $Z = 58$	
Odd configurations	4f5d6s ² , 4f5d ² 6s, 4f5d ³ , 4f ² 6s6p, 4f5d6p ² , 4f6s6p ² , 4f ² 5d6p
Even configurations	4f6s5d6p, 4f ² 6s ² , 4f6s ² 6p, 4f5d ² 6p, 4f5d ² 6p, 4f ² 6s5d, 4f ² 5d ² , 4f ² 6p ²
Pr I $Z = 59$	
Odd configurations	4f ³ 6s ² , 4f ² 5d6s6p, 4f ² 6s ² 6p, 4f ³ 5d6s, 4f ² 5d ² 6p, 4f ³ 5d ² , 4f ³ 6p ²
Even configurations	4f ² 5d6s ² , 4f ² 5d ² 6s, 4f ³ 6s6p, 4f ³ 5d6p, 4f5d ² 6s6p, 4f5d ³ 6p, 4f5d6s ² 6p

19 × 19 and 37 × 37. Every tenth element is plotted—hence the axis labels $i/10$, $j/10$. The basis states are arranged so that the diagonalized H has its H_{ii} matrix elements increasing monotonically with i . Also, the Hamiltonians are of one parity and the states with different J^π (total angular momentum and parity) do not interact with each other. It can be seen that the diagonal ‘ridge’ is more pronounced in both the ls and jj coupling schemes for even Ce than odd Ce. Note the presence of some large off-diagonal coupling matrix elements and the symmetry of the matrices. For both even and odd Ce, the ls and jj coupling matrices appear very similar.

It can be seen that the diagonal ‘ridge’ is again more pronounced in even Pr than odd Pr, for both ls and jj coupling. There are very dominant coupling matrix elements at ‘one end’ of the ridge for all of the Pr Hamiltonian matrices and there also appear to be slightly more sizeable off-diagonal elements in odd Pr than even Pr.

3. Hamiltonian matrix element distribution

Statistical information about the off-diagonal elements of the Hamiltonian matrices for the odd and even levels of Ce and Pr are presented in tables 2–5. In an earlier work on Ce [1] it states that $|\overline{H_{ij}}| \approx \sqrt{H_{ij}^2}/\sqrt{W^2}$ if the matrix elements have random signs. W is chosen as the number of elements of the ‘upper triangle’ of the matrix. This in fact can be seen to be true; for example, for Ce 4⁺ and Pr 11/2⁺, in ls coupling, the corresponding values of $\sqrt{H_{ij}^2}/\sqrt{W^2}$ are 1.5×10^{-6} and 1.8×10^{-7} eV respectively, using the whole matrix $\sqrt{H_{ij}^2}$ as in [1]. It can also be seen that in both Ce and Pr there is a consistent factor of three to four times more non-zero matrix elements in jj coupling than in ls coupling. This leads to the $ls\sqrt{H_{ij}^2}$ being almost double those of the corresponding jj cases. Whether or not these facts are a true reflection of basis state representation dependence is not known since the results in tables 2–5 are highly dependent on the output accuracy of the Cowan code. In the present study, for the Hamiltonian matrices, zero was output if $|H_{ij}| < 10^{-3}$ eV. However, for both Ce and Pr $\sqrt{H_{ij}^2}$ is consistent in both coupling schemes, i.e. ≈ 0.14 – 0.15 eV for $H_{ij} \neq 0$ and ≈ 0.04 – 0.06 eV for the whole matrix.

In both Ce and Pr, V/D (where $V = \sqrt{H_{ij}^2}$, $H_{ij} \neq 0$ only; D is the mean level spacing of the unperturbed $H_0(H_{ii})$ energy levels) in the ls coupling scheme is approximately double V/D in jj coupling; i.e., this strongly suggests basis-dependent results for the value of V . However,

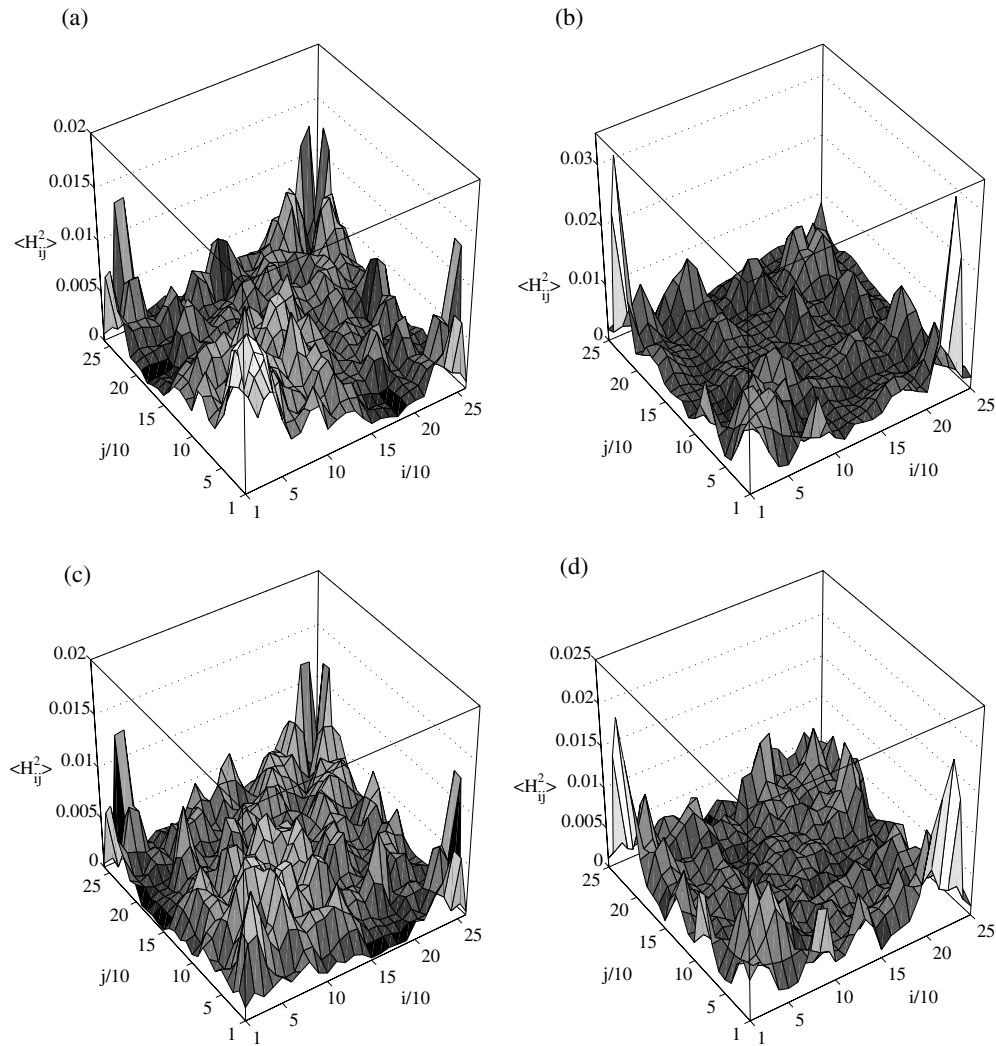


Figure 1. Window-averaged Hamiltonian matrix for (a) even Ce in *jj* coupling, (b) odd Ce in *jj* coupling, (c) even Ce in *ls* coupling and (d) odd Ce in *ls* coupling.

since the D values for both the *ls* and *jj* coupling schemes of the corresponding parity and element are very nearly the same, for example 0.034 eV for even Ce in both coupling schemes, the basis function representation is more visible for the much smaller off-diagonal elements. This indicates the prominent role of the diagonal matrix elements in these matrices. Also it is found that V/D is very approximately double the corresponding value in Pr compared with that of Ce, for both *ls* and *jj* coupling. Since $V/D \gg 1$ this would suggest strong perturbation of the unperturbed Hamiltonian. However, again, the accuracy of the Cowan output must be taken into consideration.

The distributions of all the even and odd Ce and Pr off-diagonal H_{ij} elements can be approximated by the exponential [1]

$$\frac{\Delta N}{\Delta H} \propto |H_{ij}|^{-1/2} \exp\left(\frac{-|H_{ij}|}{V}\right) \quad (3)$$

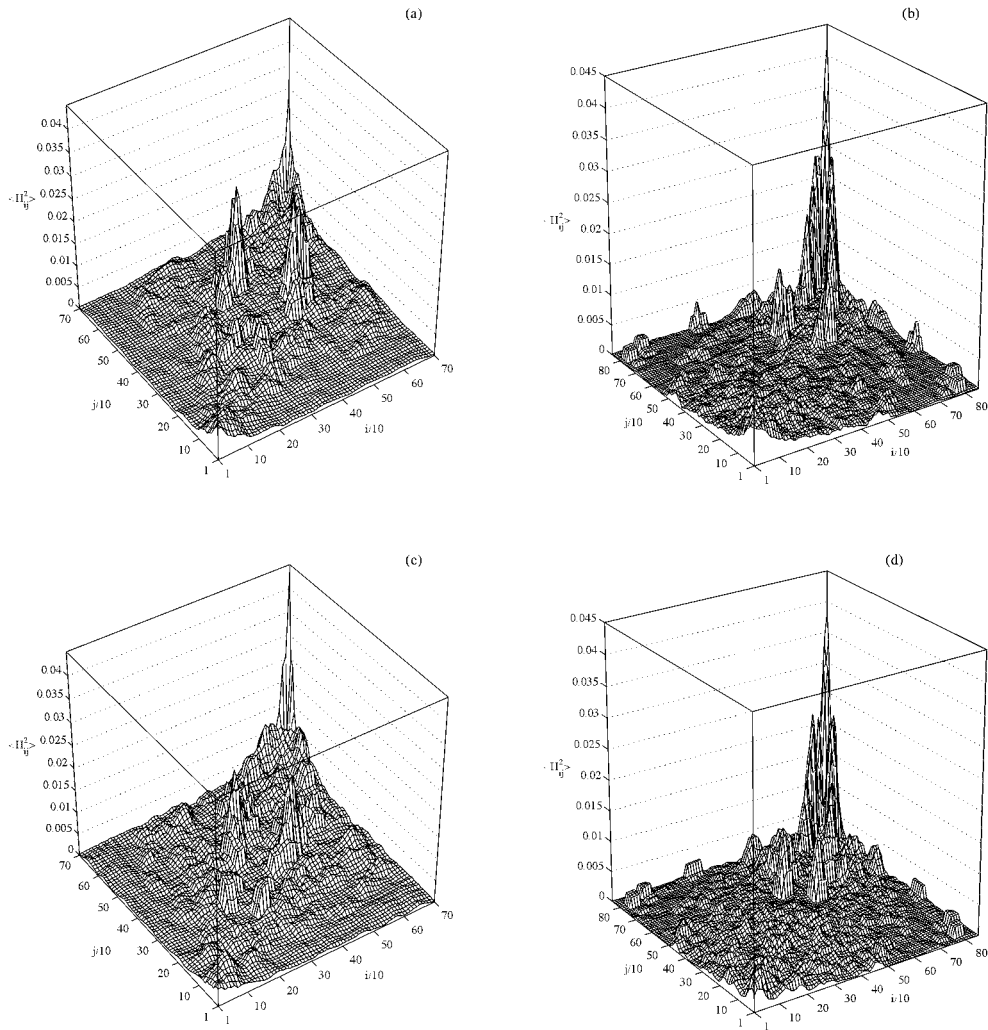


Figure 2. Window-averaged Hamiltonian matrix for (a) even Pr in *jj* coupling, (b) odd Pr in *jj* coupling, (c) even Pr in *ls* coupling and (d) odd Pr in *ls* coupling.

as shown by the logarithmic plots in figures 3 and 4. In fact the following function, with fitting parameters α and β , was used for the curve fitting of the off-diagonal H_{ij} elements:

$$F(x, \alpha, \beta) = \alpha(|x|^{-1/2})e^{-\frac{|x|}{\beta}} \quad (4)$$

α and β for the least-squares fitting of the non-zero H_{ij} are given in tables 6 and 7 for Ce and Pr respectively. Note that the respective values of β are fairly consistent with the corresponding values of $\sqrt{H_{ij}^2}$ ($H_{ij} \neq 0$ only) as shown in tables 2–5.

It can be seen from the logarithm of $F(H_{ij}, \alpha, \beta)$ versus H_{ij} that there is a large number of small matrix elements since the matrix element between two configurations vanishes if they contain more than two different orbitals. This exponential distribution appears to be generic for many-body systems [1]. Figures 3 and 4 also show the apparent presence of more non-zero elements in *jj* than *ls* coupling.

Table 2. Statistical characteristics of the off-diagonal Hamiltonian matrix elements of even Ce I in *ls* and *jj* coupling.

	Ce even <i>ls</i>		Ce even <i>jj</i>	
	Whole matrix	$H_{ij} \neq 0$ only	Whole matrix	$H_{ij} \neq 0$ only
$\overline{H_{ij}^2}$ (eV ²)	0.0035	0.022	0.0039	0.0061
$\sqrt{\overline{H_{ij}^2}}$ (eV)	0.0595	0.1472	0.0628	0.078
$\overline{H_{ij}}$ (eV)	-7.1×10^{-4}	-4.2×10^{-3}	-1.2×10^{-3}	-1.82×10^{-3}
No. of H_{ij} ($i < j$)	37 950	6209	37 950	24 632
Matrix dimension	276 × 276			
D (eV)	0.0343		0.0336	
$\frac{V}{D}$	4.29		2.32	

Table 3. Statistical characteristics of the off-diagonal Hamiltonian matrix elements of odd Ce I in *ls* and *jj* coupling.

	Ce odd <i>ls</i>		Ce odd <i>jj</i>	
	Whole matrix	$H_{ij} \neq 0$ only	Whole matrix	$H_{ij} \neq 0$ only
$\overline{H_{ij}^2}$ (eV ²)	0.0038	0.023	0.0042	0.0071
$\sqrt{\overline{H_{ij}^2}}$ (eV)	0.062	0.1529	0.0653	0.0842
$\overline{H_{ij}}$ (eV)	-9.8×10^{-6}	-5.96×10^{-6}	-5.2×10^{-4}	-8.5×10^{-4}
No. of H_{ij} ($i < j$)	33 670	5537	33 670	20 220
Matrix dimension	260 × 260			
D (eV)	0.0393		0.0385	
$\frac{V}{D}$	3.89		2.19	

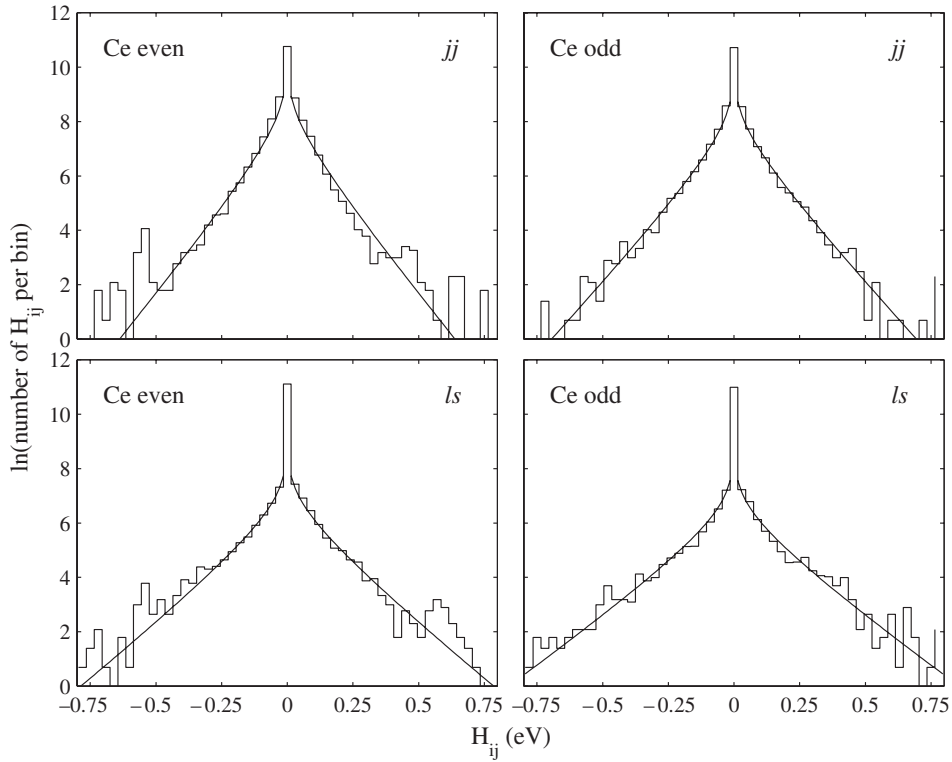
Table 4. Statistical characteristics of the off-diagonal Hamiltonian matrix elements of even Pr I in *ls* and *jj* coupling.

	Pr even <i>ls</i>		Pr even <i>jj</i>	
	Whole matrix	$H_{ij} \neq 0$ only	Whole matrix	$H_{ij} \neq 0$ only
$\overline{H_{ij}^2}$ (eV ²)	0.0024	0.022	0.0026	0.0073
$\sqrt{\overline{H_{ij}^2}}$ (eV)	0.0492	0.1484	0.0512	0.0857
$\overline{H_{ij}}$ (eV)	7.15×10^{-5}	6.50×10^{-4}	-2.15×10^{-4}	-6.03×10^{-4}
No. of H_{ij} ($i < j$)	271 216	29 816	271 216	96 537
Matrix dimension	737 × 737			
D (eV)	0.0158		0.0149	
$\frac{V}{D}$	9.45		5.75	

Equation (3) in fact implies that the distributed quantities in the realistic case are not the off-diagonal Gaussian random matrix elements but rather some quantities resembling square roots of them [1]. The underlying physical reason might be related to the presence of multipole–multipole forces; however, the Coulomb interaction in an atom is determined by a small number of low multipoles [4].

Table 5. Statistical characteristics of the off-diagonal Hamiltonian matrix elements of odd Pr I in ls and jj coupling.

	Pr odd ls		Pr odd jj	
	Whole matrix	$H_{ij} \neq 0$ only	Whole matrix	$H_{ij} \neq 0$ only
$\overline{H_{ij}^2}$ (eV ²)	0.0016	0.016	0.0017	0.0039
$\sqrt{\overline{H_{ij}^2}}$ (eV)	0.0404	0.1246	0.042	0.0623
$\overline{H_{ij}}$ (eV)	4.3×10^{-6}	4.1×10^{-5}	-2.1×10^{-4}	-4.6×10^{-4}
No. of H_{ij} ($i < j$)	392 941	41 327	392 941	178 154
Matrix dimension	887×887			
D (eV)	0.0130		0.0130	
V	9.58		4.79	
$\frac{V}{D}$	9.58		4.79	

**Figure 3.** The distribution of the off-diagonal elements of the Ce Hamilton matrix. The solid curve is given by equation (4).

In order to numerically show the bandedness of the matrices, as opposed to the visual impressions of figures 1 and 2, the following ‘statistical tests’ were also applied to the Hamiltonian matrix elements as performed by Gribakina *et al* [2].

- Dependence of H_{ij} on their distance from the diagonal.
- Sparsity of the H_{ij} .
- The average of the squared non-zero matrix elements at a given distance from the diagonal.

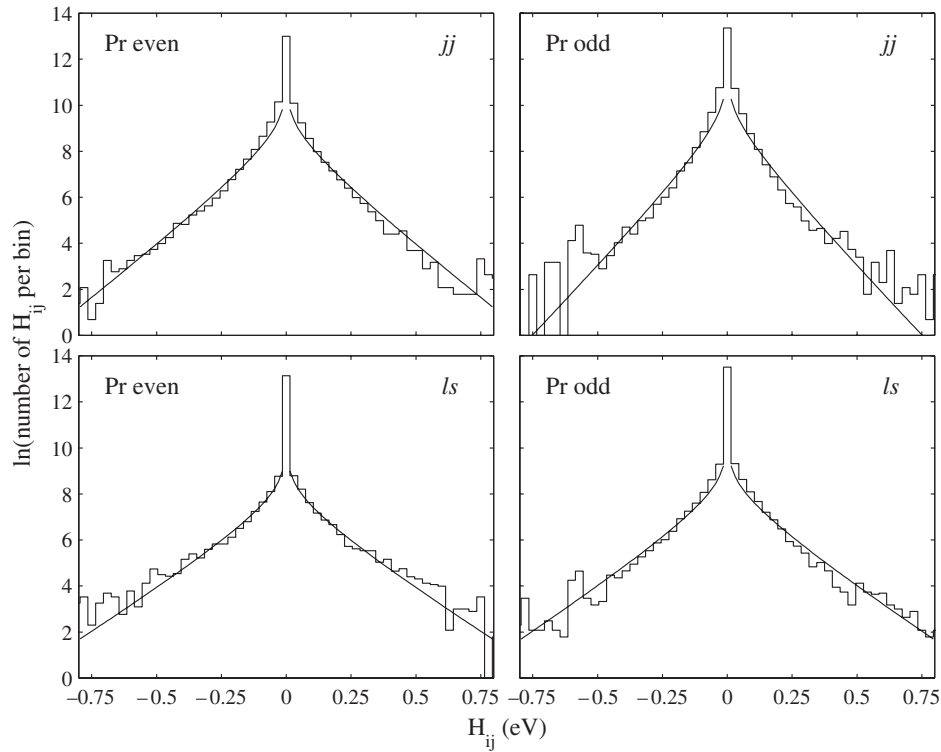


Figure 4. The distribution of the off-diagonal elements of the Pr Hamilton matrix.

Table 6. Various curve fitting parameters for even and odd Ce.

	Ce even		Ce odd	
	<i>ls</i>	<i>jj</i>	<i>ls</i>	<i>jj</i>
α	314.4	1107.3	260.74	876.64
β	0.134	0.088	0.152	0.099
k	7.68×10^{-4}	-4.28×10^{-4}	7.199×10^{-4}	-9.57×10^{-5}
S_0	0.24	0.612	0.233	0.595
H_0	0.216	0.188	0.239	0.200
b	116.62	52.74	152.12	60.20
$\overline{\Delta E}$ (eV)	1.87	1.86	2.24	2.11
$\frac{\Delta E}{D}$	55	55	57	54

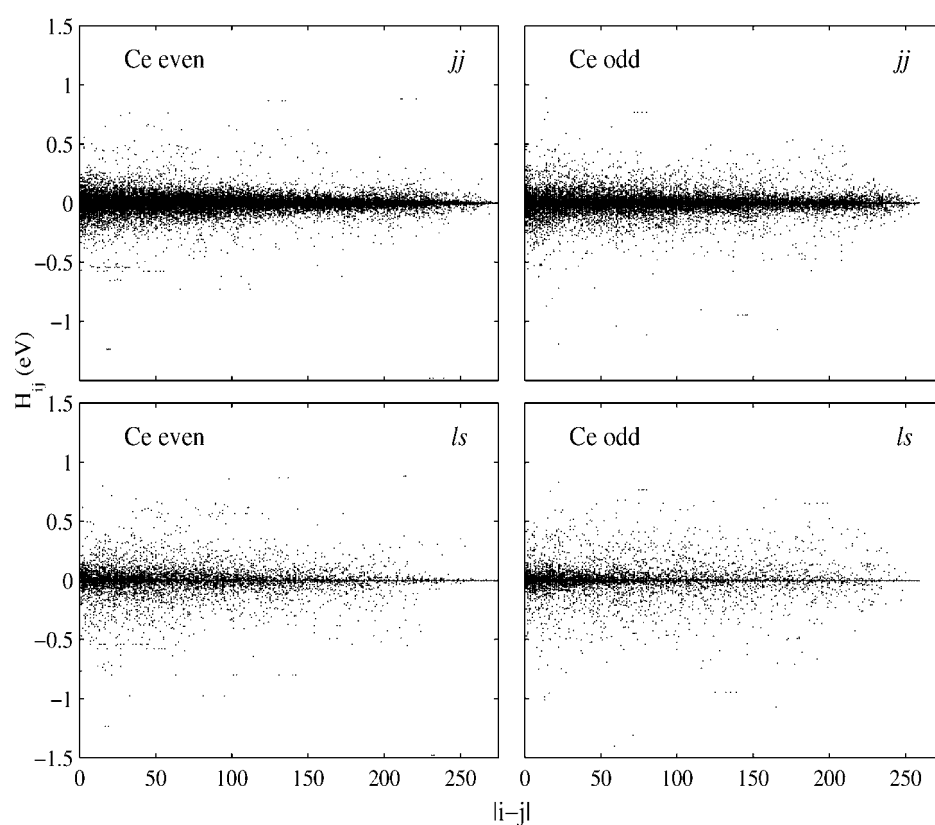
The dependences of H_{ij} on their distance from the diagonal $\Delta = |i - j|$ are shown in figures 5 and 6. One can see that the matrix elements H_{ij} decrease in magnitude as $|i - j|$ increases. Also, the matrix elements appear more dispersed in *ls* than *jj* coupling for both even and odd Ce and Pr. Note the presence of large off-diagonal elements in both Ce and Pr and in both coupling schemes.

Figures 7 and 8 present the sparsity as defined in [2]

$$\text{sparsity } S = \frac{\text{number of } |H_{ij}| \neq 0}{\text{number of all } H_{ij}} \quad |i - j| \text{ fixed.} \quad (5)$$

Table 7. Various curve fitting parameters for even and odd Pr.

	Pr even		Pr odd	
	<i>ls</i>	<i>jj</i>	<i>ls</i>	<i>jj</i>
α	1086.6	2563.5	1374.0	4188.6
β	0.147	0.118	0.141	0.088
k	1.36×10^{-4}	-4.72×10^{-4}	1.48×10^{-4}	-1.45×10^{-5}
S_0	0.146	0.242	0.151	0.45
H_0	0.226	0.172	0.184	0.115
b	254.20	155.69	255.17	192.26
$\overline{\Delta E}$ (eV)	2.33	2.25	1.68	1.71
$\frac{\overline{\Delta E}}{D}$	146	140	129	132

**Figure 5.** Matrix elements H_{ij} (eV) of Ce as a function of the distance to the main diagonal $|i - j|$.

Note that this definition of sparsity is based on the number of non-zero elements as opposed to the number of elements that are zero valued.

For Ce and Pr in the *jj* coupling scheme the sparsity either tends to increase or is approximately constant and then ‘diverges’, whereas in the *ls* coupling cases, for Ce and Pr, there is a definite decrease in sparsity. It can also be seen that the sparsity is greater in the

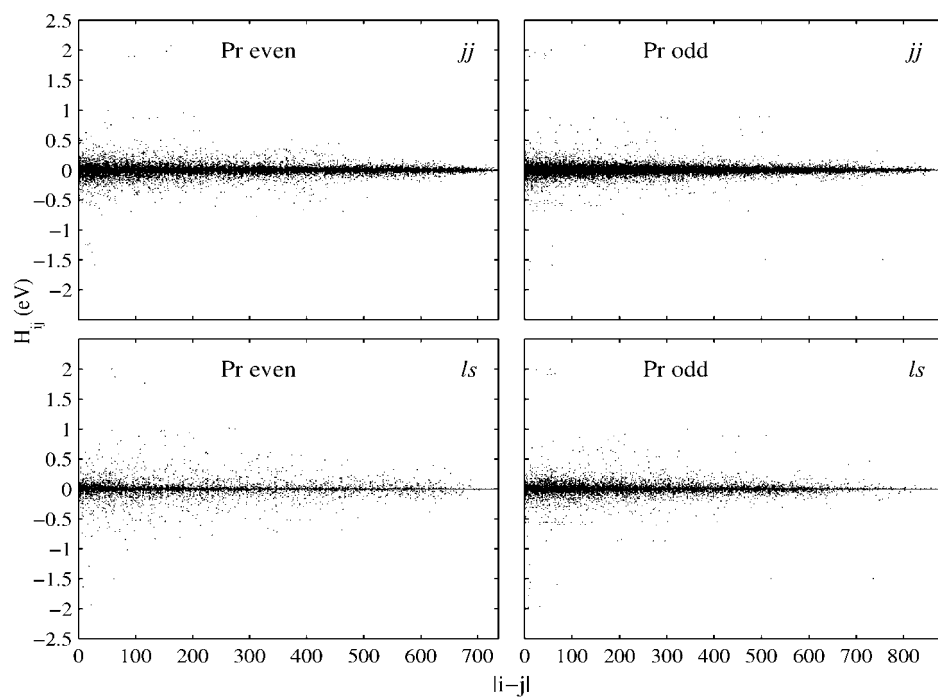


Figure 6. Matrix elements H_{ij} (eV) of Pr as a function of the distance to the main diagonal $|i - j|$.

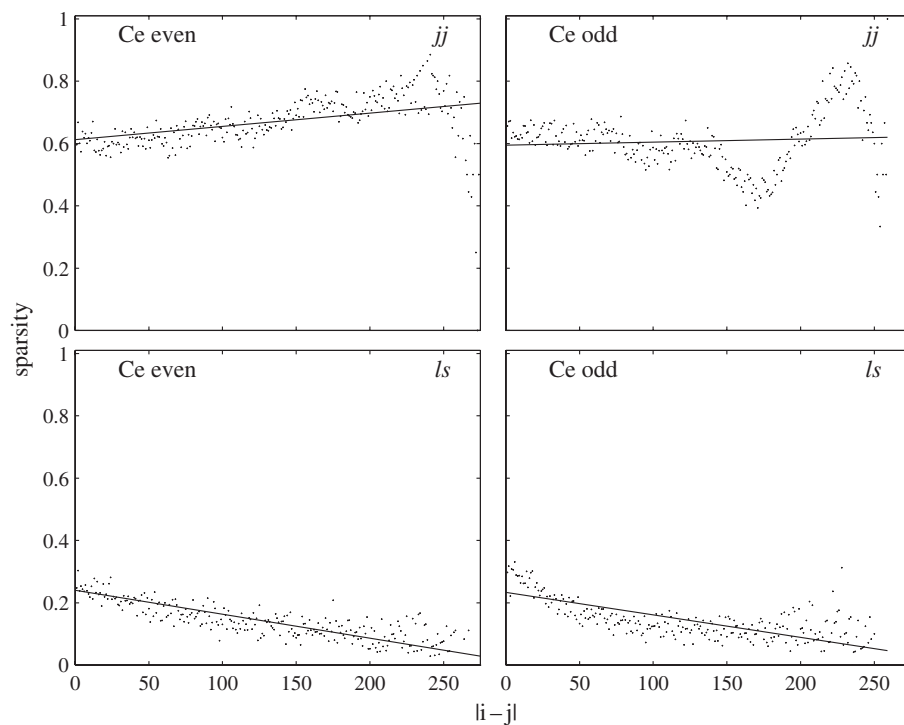


Figure 7. Sparsity S of the Ce Hamiltonian matrix.

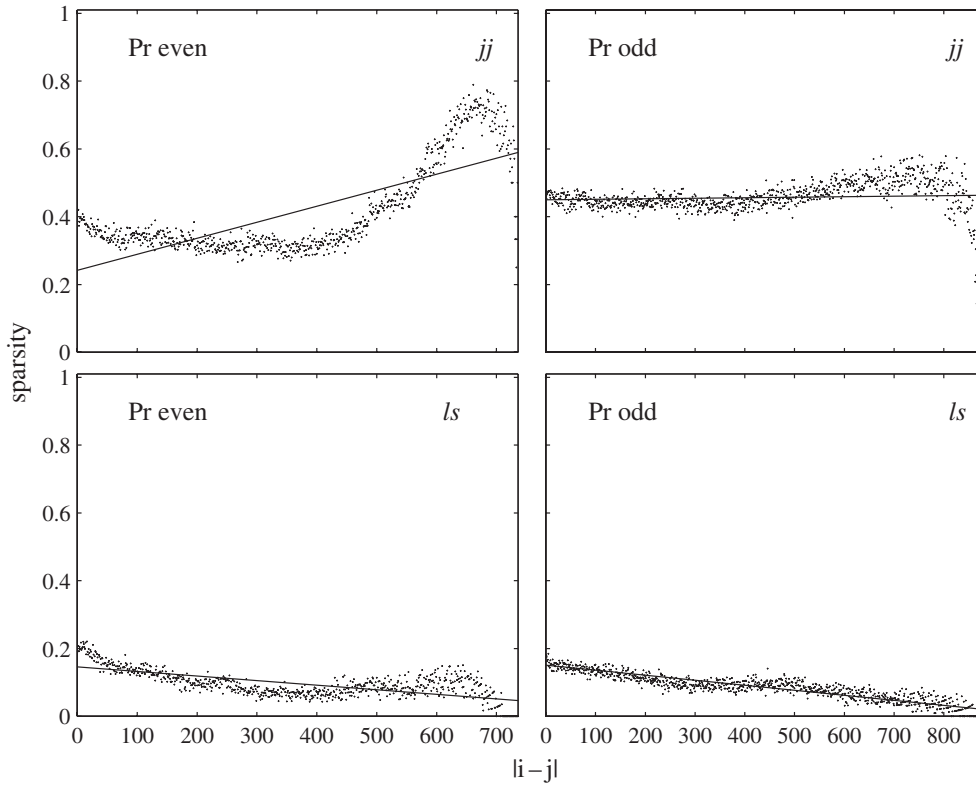


Figure 8. Sparsity S of the Pr Hamiltonian matrix.

jj coupling for both Ce and Pr than in ls coupling. The ‘sparsity’ is fitted according to [2]:

$$S(\Delta) = S_0 - k\Delta. \quad (6)$$

Parameters of the fit, S_0 and k , are given in tables 6 and 7. For the jj coupling scheme this form for $S(\Delta)$ is only appropriate up to $\Delta \approx 150$ for Ce and up to $\Delta \approx 400$ for Pr. k is very small for both Ce and Pr.

In order to estimate the number bandwidth b , the mean squared matrix elements were fitted according to [2]

$$\langle H_{ij}^2 \rangle_{|i-j|=\Delta} = H_0^2 \exp\left(-\frac{\Delta}{b}\right) \quad (7)$$

where $\langle H_{ij}^2 \rangle_{|i-j|=\Delta}$ is the average of the squared non-zero matrix elements at a given distance Δ from the diagonal. The dependence of $\langle H_{ij}^2 \rangle_{|i-j|=\Delta}$ on Δ for Ce and Pr are shown in figures 9 and 10. The values of b as shown in tables 6 and 7 are smaller than N (the matrix dimension) by factors of 2 to 3 for ls coupling and by factors of 4 to 5 for jj coupling, which indicates that for both Ce and Pr not only are the matrices banded but the bands are larger for ls coupling than jj coupling, as is seen in figures 1 and 2. However, $\langle H_{ij}^2 \rangle^{1/2}$ shows a ‘better fit’ to the previous equation for jj coupling in both Ce and Pr and there appears to be relatively more ‘scatter’ in all of the ls graphs. Again, note the presence of the coupling of distant matrix elements.

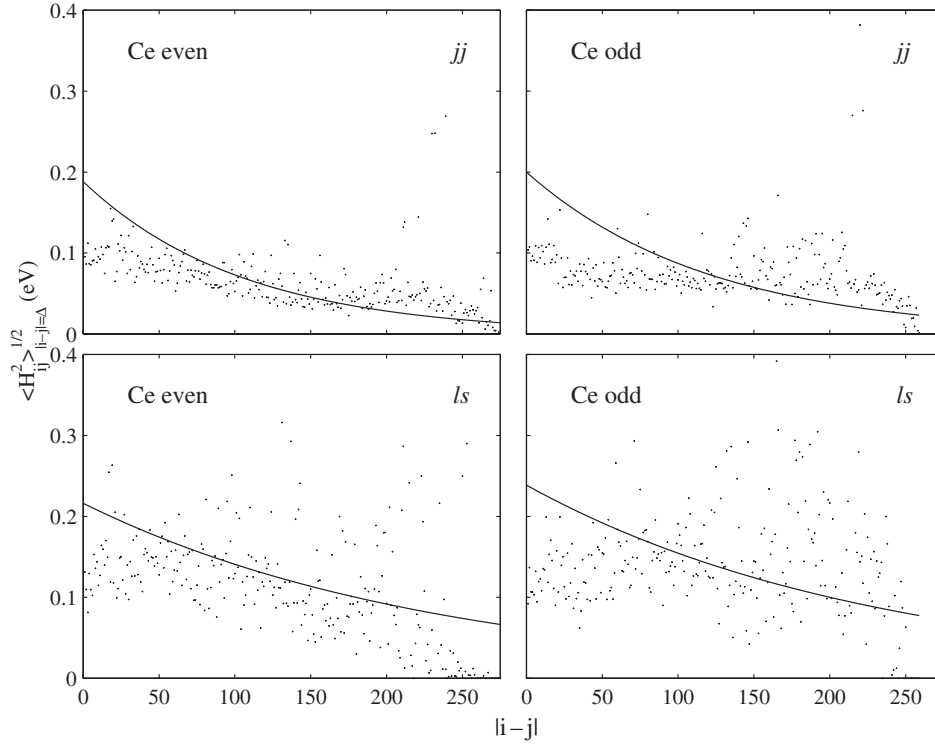


Figure 9. Root mean squared matrix elements as a function of the distance to the main diagonal for the Ce Hamiltonian matrix.

Figures 11 and 12 show the energy bandwidths ΔE_i calculated according to [1,2]

$$(\Delta E_i)^2 = \frac{\sum_j (H_{ii} - H_{ij})^2 |H_{ij}|^2}{\sum_{j \neq i} |H_{ij}|^2}. \quad (8)$$

In all cases there are large fluctuations in ΔE_i . Also shown are the local averages (± 9 for Ce, ± 18 for Pr) which display a relatively slow dependence on i . In fact the running averaged energy bandwidths are quite constant for odd Pr in both ls and jj coupling. The overall mean energy bandwidths $\overline{\Delta E}$ (as indicated by the dashed lines in the figures) are shown in tables 6 and 7, along with the number bandwidths as calculated via $b = \overline{\Delta E}/D$, where D is the mean level spacing of the unperturbed energy levels. $\overline{\Delta E}/D$ is approximately half that of the b calculated via $\langle H_{ij}^2 \rangle$ for ls coupling, whereas $\overline{\Delta E}/D$ is of the same order as b in jj coupling. This occurs for both parities of Ce and Pr. All of the $\overline{\Delta E}$ are very similar in value in both Ce and Pr at approximately 1.7–2.3 eV. Note that all of the previous results are again highly dependent on the output accuracy of the Cowan code.

4. Structure of eigenstates and basis states

Examples of energy eigenstates $|j\rangle$, with components C_i in a basis $|i\rangle$, and basis states, with components C_j in a basis $|j\rangle$, for Pr are shown in figures 13–20. The energy scales are all given with respect to zero. One can see that even relatively low-lying eigenstates are distributed among a large number of component basis states. This is also true for the basis

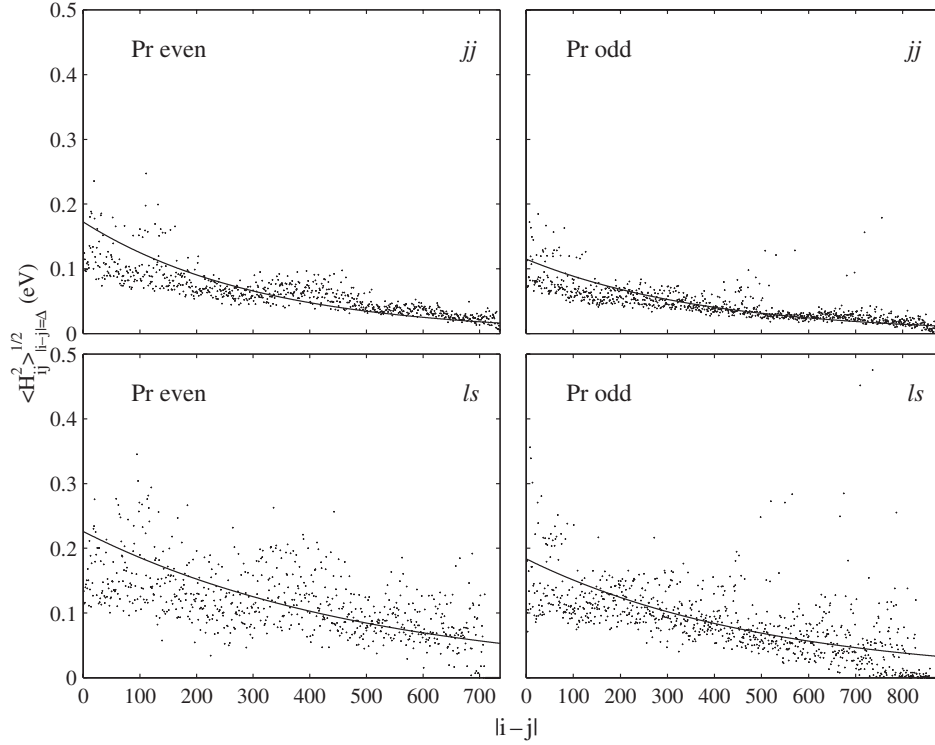


Figure 10. Root mean squared matrix elements for the Pr Hamiltonian matrix.

states as a function of $|j\rangle$. In fact the energy eigenstates are compound states [1]—compound states are energy eigenvectors composed of a large number of simple basis states; for example, compound nuclear states have 10^4 – 10^6 principal components. The eigenstates of both Ce and Pr are found to be more localized in the middle of the spectrum than at the upper and lower bounds. There is also a general trend for the energy centres of the eigenstates to increase as the energy of the eigenstate increases. This is also true of the basis states as a function of $|j\rangle$. The corresponding eigenstates appear to be quite similar in both ls and jj coupling for both Ce and Pr. This is because the corresponding Hamiltonian matrices are quite similar and consequently the matrices that diagonalize them are comparable.

The $|\text{amplitude}|^2$ is now considered, i.e. $W_i^j = |C_i^j|^2$, where the subscripts refer to the basis states and the superscripts correspond to the (compound) eigenstates. Thus the structure is given by the dependence of W_i^j on i for fixed values of j . This gives rise to the shape of an eigenfunction (EF), whereas fixing i and varying j gives rise to the local density of states (LDOS). The LDOS gives information about the spread of the energy, initially concentrated in a specific basis state $|i\rangle$, when the perturbation is ‘switched on’. The envelope of this function W_i^j , in the energy representation, is known as the strength function or local spectral density of states [12].

The spectral density of states (LDOS) for an unperturbed state $|i\rangle$ is defined as

$$w_i(E) = \sum_j |C_{ij}|^2 \delta(E - E_j) \quad (9)$$

where E_j is the eigenenergy of the perturbed eigenstate $|j\rangle$ and $C_{ij} = \langle i|j\rangle$. The function $w_i(E)$ is also known as the ‘strength function’ or ‘Green spectra’ [5]. The form of the LDOS

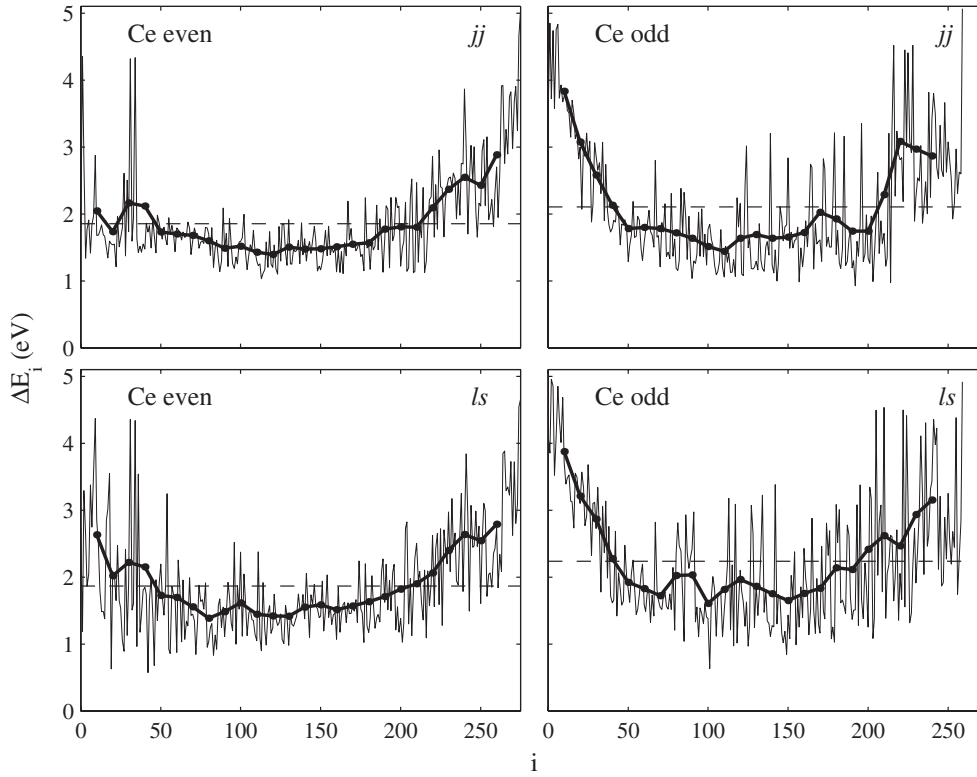


Figure 11. Energy bandwidths of the Ce Hamiltonian matrix.

for band random matrices has been analytically studied by Wigner [13, 14]. Particularly, it was shown that when the perturbation is not large the LDOS has the form

$$w_{\text{BW}}(E - E_i^o) = \frac{\Gamma/2\pi}{(E - E_i^o)^2 + \Gamma^2/4} \quad (10)$$

which is also known as the Breit–Wigner (BW) law. Here, Γ is the full width at half maximum (FWHM) of the distribution. The BW form for the strength function is an immediate consequence of the assumption of constant coupling between matrix elements [15]. For larger perturbations, the form of the LDOS becomes model dependent and in the intermediate region can be approximately described by a Gaussian distribution [5]. It should be noted that one of the first studies that systematically addressed the issues of the LDOS, after the earlier work by Wigner [13, 14], and its various shapes ranging from Lorentzian to Gaussian depending on the interplay between sparsity, bandedness and the average increase of entries along the main diagonal, was an analytical study by Fyodorov *et al* [5].

The shape of EFs is defined as

$$w_j(E^o) = \sum_i |C_{ij}|^2 \delta(E^o - E_i^o) \quad (11)$$

in the unperturbed energy basis. The mean squared components $\langle |C_{ij}|^2 \rangle$ were calculated and, in order to suppress fluctuations, window averages of ± 9 for Ce and ± 18 for Pr were used. In fact, if the spectrum is very dense, it becomes appropriate to consider a continuous LDOS or EF function, representing the ‘strength’ per unit energy, and obtained by averaging over the

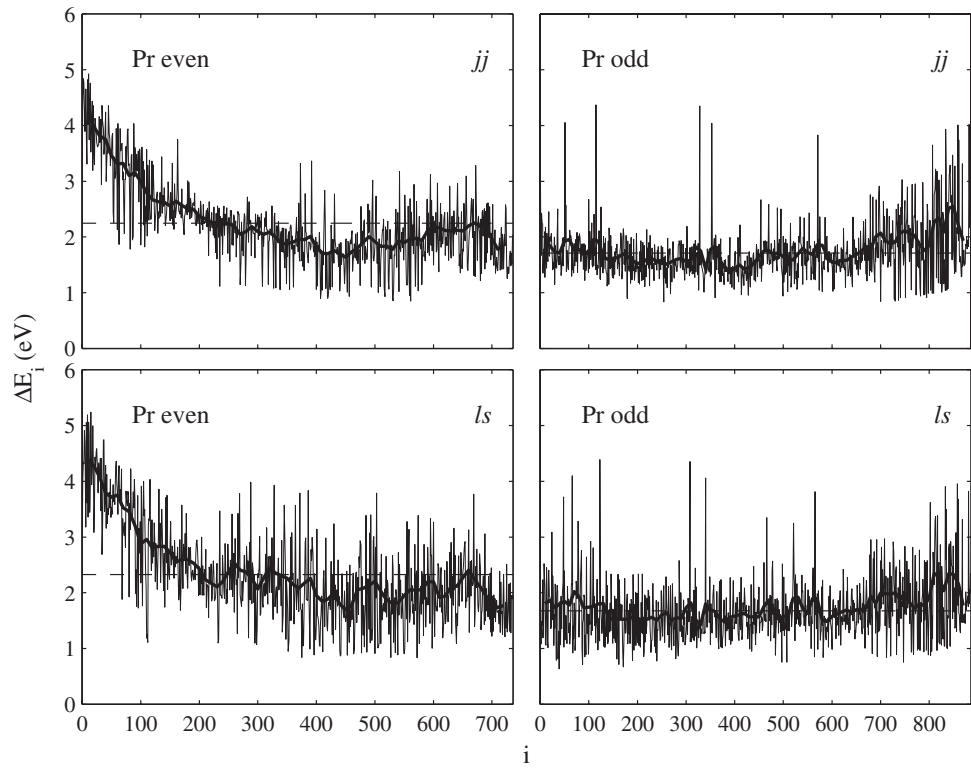


Figure 12. Energy bandwidths of the Pr Hamiltonian matrix.

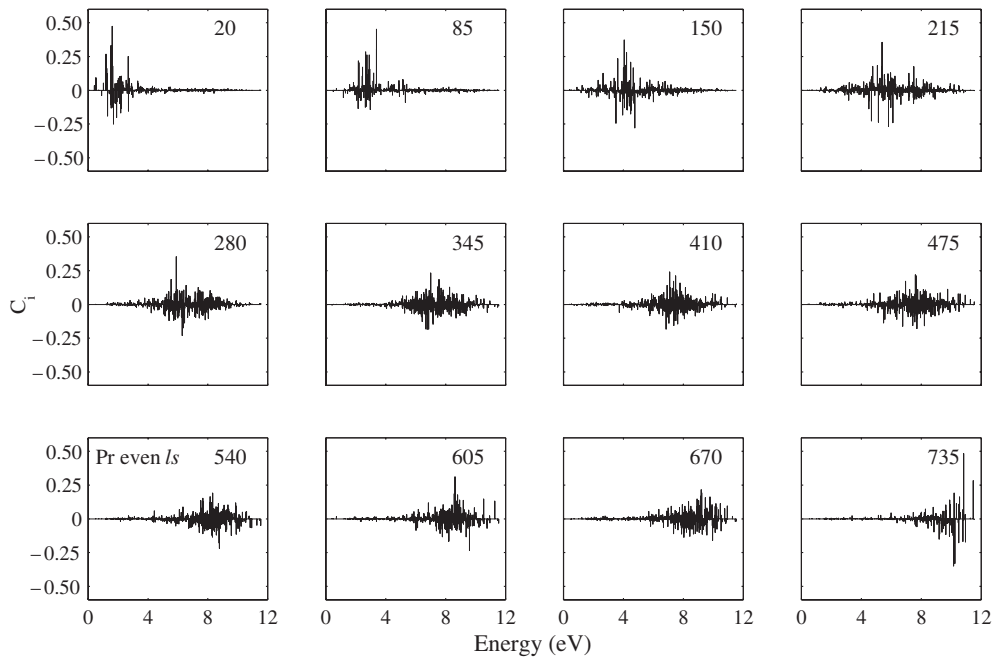


Figure 13. Various eigenstates of even Pr in ls coupling. The eigenstate components C_i are shown as a function of the basis state energies.

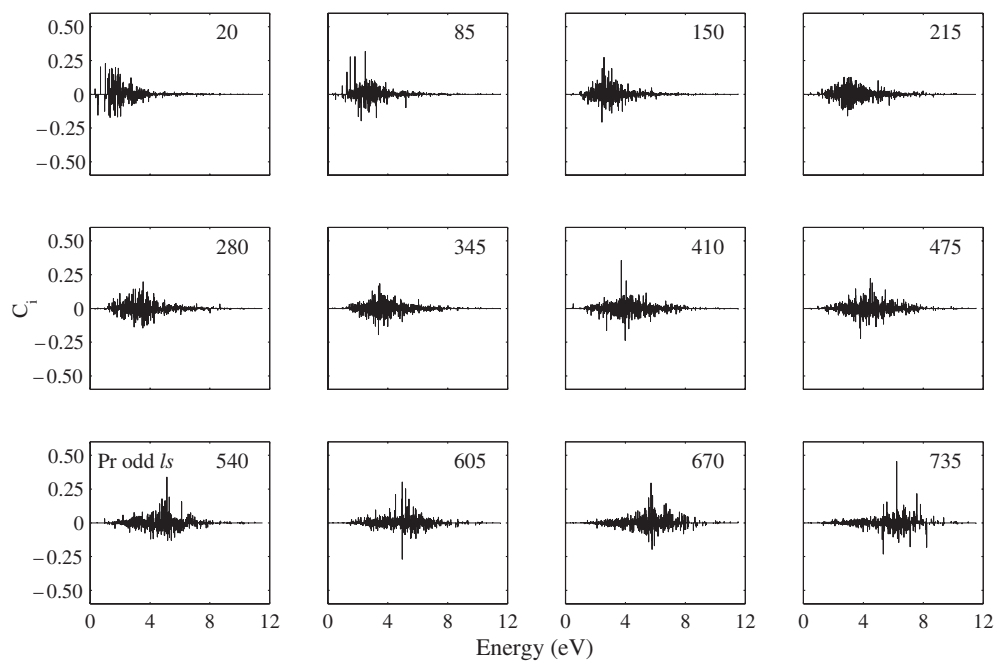


Figure 14. Various eigenstates of odd Pr in ls coupling.

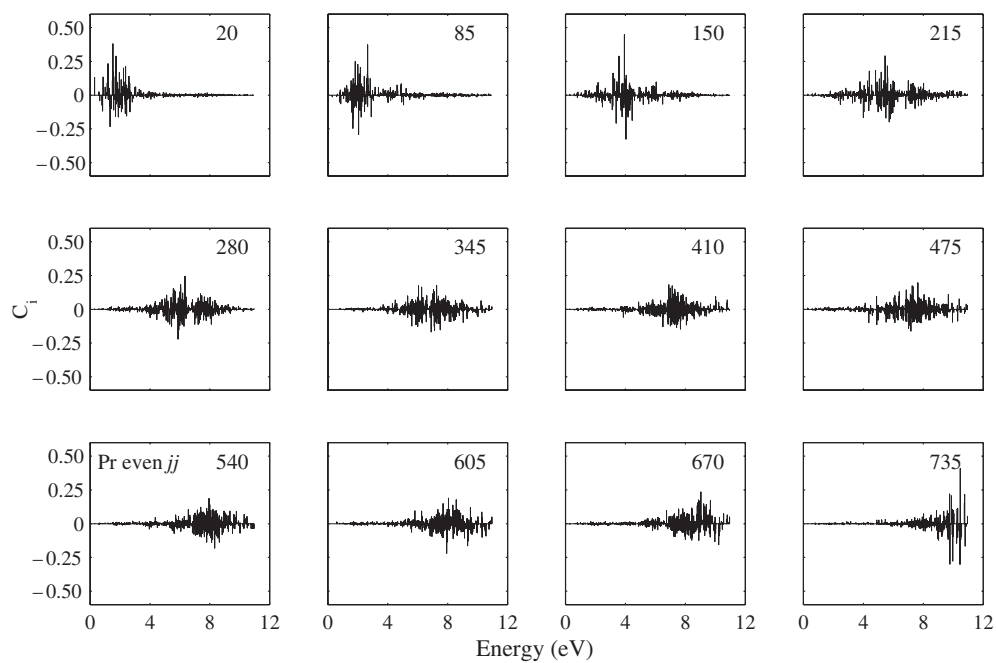


Figure 15. Various eigenstates of even Pr in jj coupling.

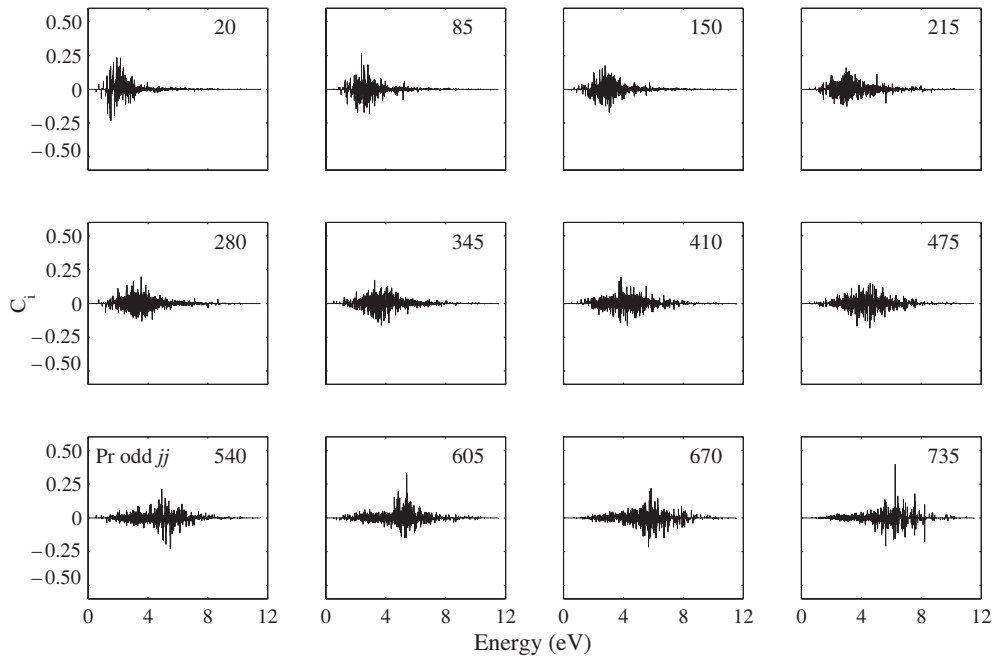


Figure 16. Various eigenstates of odd Pr in jj coupling.

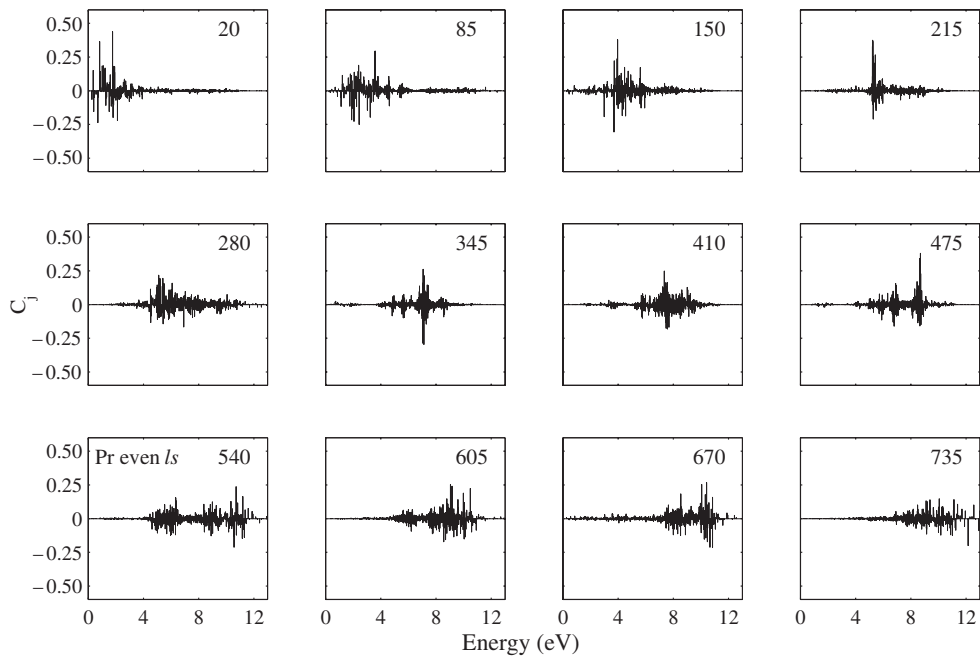


Figure 17. Various basis states of even Pr in ls coupling. The basis state components C_j are shown as a function of the eigenstate energies.

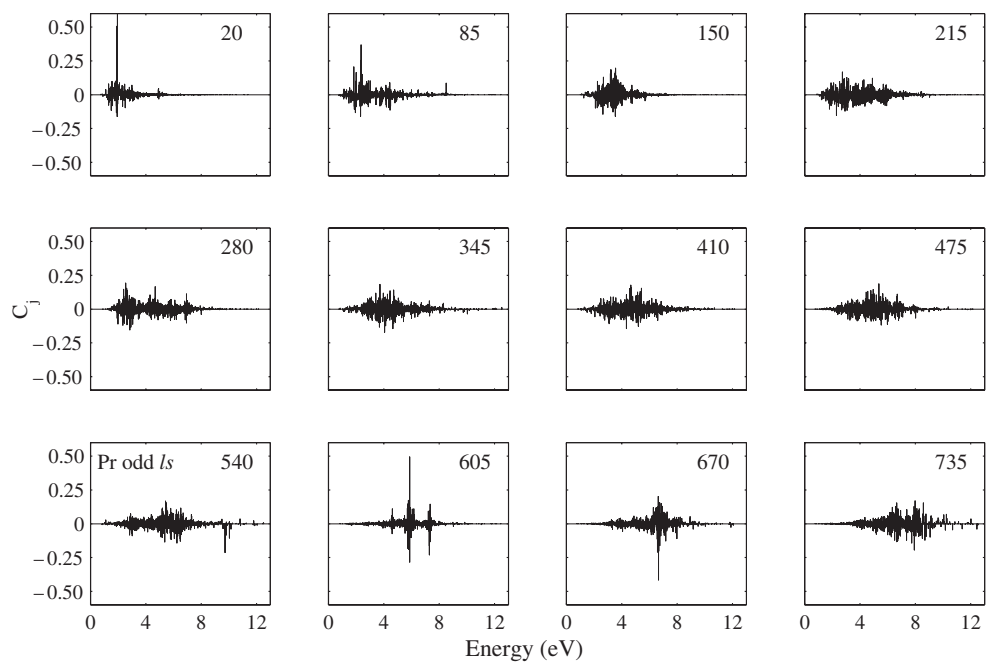


Figure 18. Various basis states of odd Pr in ls coupling.

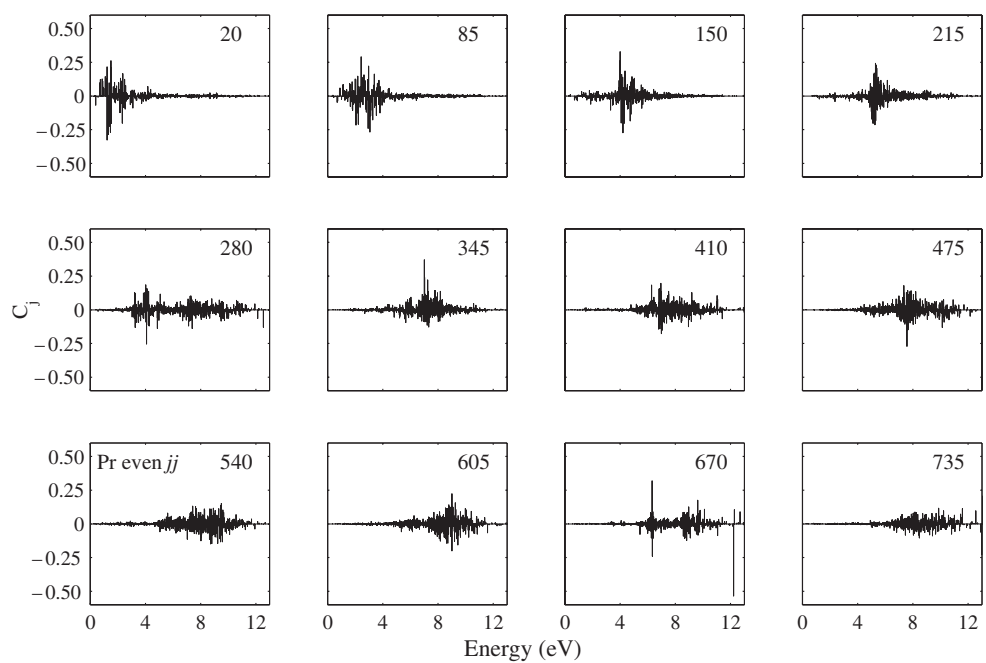


Figure 19. Various basis states of even Pr in jj coupling.

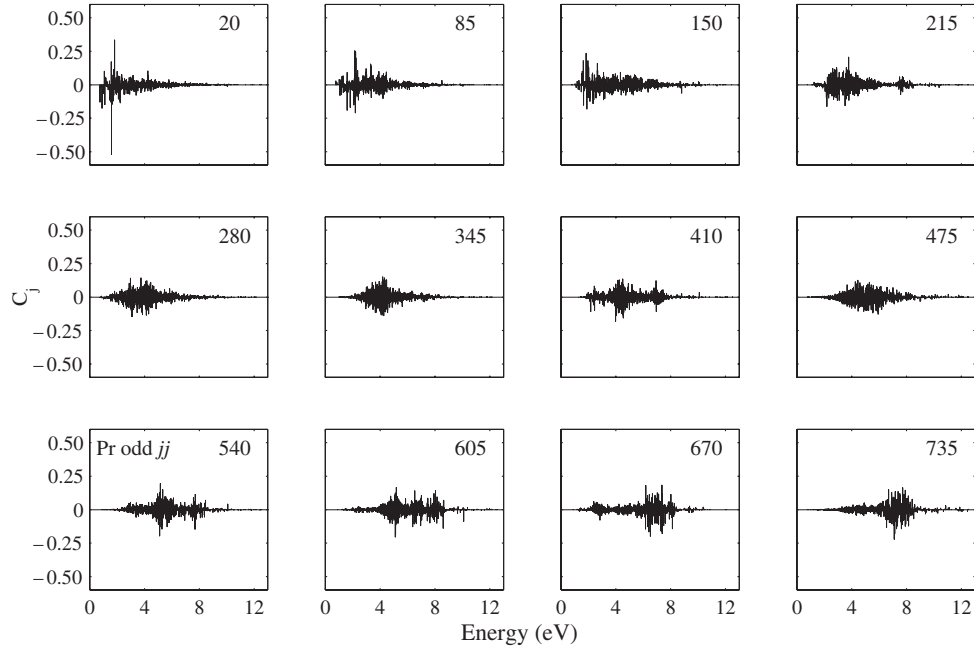


Figure 20. Various basis states of odd Pr in jj coupling.

states in a small energy interval around E . Before averaging, $w_i(E)$ and $w_j(E)$ are expressed with respect to their centroids. For the LDOS, the centroid of $w_i(E)$ is

$$E_i^o = \sum_j E_j |C_{ij}|^2 \quad (12)$$

so the LDOS can be expressed as $w_i(E - E_i^o)$. On the other hand, the centroid of $w_j(E^o)$, e_j , is defined by

$$e_j = \sum_i E_i^o |C_{ij}|^2 \quad (13)$$

and w_j can be expressed as a function of the shift ($E^o - e_j$).

The shapes of the LDOS and EF are found to be quite similar in appearance and also show the presence of localization. This is interesting since in [5, Wang *et al*]—a three-orbital schematic shell model—with increasing perturbation the shapes of the LDOS and EFs begin to deviate from each other. Note, also, that in [5, Wang *et al*] the LDOS and EFs are re-scaled in energy in order to allow for a more meaningful comparison.

The LDOS and EFs had the following functions fitted to them [1]:

$$w(E_i; E + \Delta E, \Gamma, N) = N^{-1} f(\varepsilon) \quad (14)$$

where the shape function $f(\varepsilon)$ has the following forms for various distributions:

$$\begin{aligned} f(\varepsilon) &= (1 + 4\varepsilon^2)^{-1} && \text{Lorentzian} \\ f(\varepsilon) &= (1 + 4\varepsilon^2)^{-2} && \text{Squared Lorentzian} \\ f(\varepsilon) &= \exp\left(1 - \sqrt{1 + 4\varepsilon^2}\right) && \text{Interpolation exponential} \\ f(x, d_0, \Delta E) &= \frac{1}{\sqrt{2\pi d_0^2}} e^{-\frac{(x-\Delta E)^2}{2d_0^2}} && \text{Gaussian} \end{aligned}$$

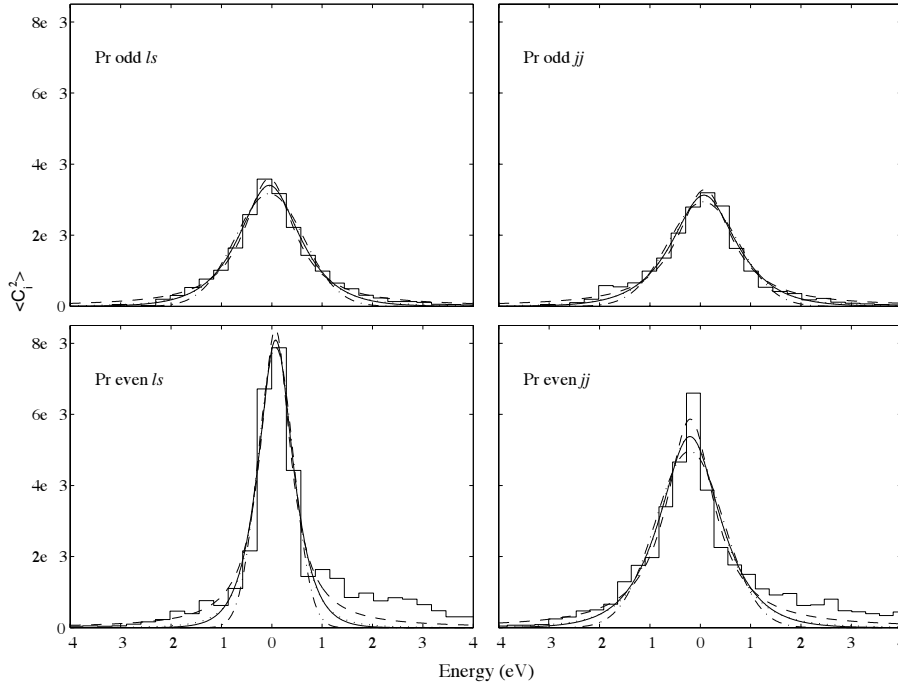


Figure 21. Selected window-averaged EFs for Pr and least-squares fitting to (i) Lorentzian (dashed), (ii) squared Lorentzian (dotted), (iii) interpolation exponential (solid) and (iv) Gaussian (dash-dot).

where $\varepsilon = (E_i - E - \Delta E)/\Gamma$, N is the number of principal components, Γ is the FWHM and the displacement of the maximum is allowed for by a parameter ΔE . The number of principal components indicates the number of components that contribute significantly to a given eigenstate (basis state). Note that the Lorentzian has the form

$$f\left(\frac{E_i - E - \Delta E}{\Gamma}\right) = \frac{\Gamma^2}{4(E_i - E - \Delta E)^2 + \Gamma^2}. \quad (15)$$

As a qualitative guide to the ‘goodness of fits’, the sum of the squares of the residuals (SSR) was calculated using a nonlinear least-squares Marquardt–Levenberg algorithm. The functions were all fitted between ≈ -3.5 and 3.5 eV. In general it was found that the Lorentzian function has the lowest SSR for each state. This was more obvious in the SSR for the LDOS and EFs of Pr of both parities and both coupling schemes. It was also observed that the squared Lorentzian and interpolation exponential have very similar SSRs, whereas the Gaussian fits had the greatest SSR. Thus the Lorentzian gives the ‘best fit’. Typical window-averaged EFs and LDOS with the least-squares fitted functions are shown in figures 21–24 for Pr. The 232nd and 332nd states are shown for odd and even Pr respectively. These states are shown for both coupling schemes. However, the semi-logarithmic plots in figures 22 and 24 show the divergence of the fits in the tails of the LDOS and EFs. The localization of eigenstates as seen in the EFs (and correspondingly in the LDOS) implies that a perturbation mixes the basis states locally and the components of a given eigenstate rapidly vanish as one moves away from the ‘centre’ of the eigenstate. The tails indicate the coupling of distant matrix elements. Also notice that, in general, the LDOS and EFs are skewed at low and high states, but are more symmetric in the middle of the spectra. This is partly due to the low states being bounded from below, i.e. in a finite basis the very low and very high basis states cannot achieve the same

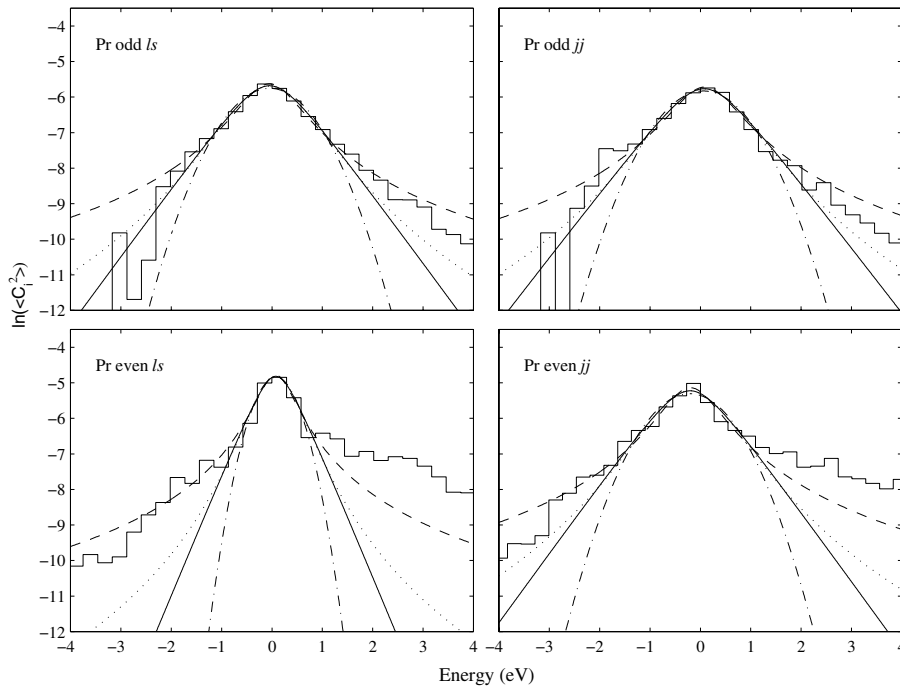


Figure 22. Selected window-averaged EFs for Pr with a semi-logarithmic scale.

degree of coupling—on average they are only coupled to $\approx b$ basis states, unlike the ‘middle’ states, which can couple to $\approx 2b$ basis states. This range of coupling (i.e. the bandedness of the Hamiltonian matrix) results in the localization of the EFs and the LDOS. The $\langle |C|^2 \rangle$ are smaller in the ‘middle’ of the spectra, indicating that the C_{ij} are more delocalized over the basis states/eigenstates than the high or low spectral regions. It also appears that the window-averaged LDOS and EF histograms are of a similar appearance in the ‘middle’ of the spectrum.

The number of principal components, N , calculated for the various $f(\varepsilon)$ distributions is shown in figures 25 and 26 for Ce and in figures 27 and 28 for Pr. It can be seen that N reaches a maximum of approximately 100 (roughly one-third of the number of available states) for Ce and approximately 300–400 for Pr (roughly one-half of the number of available states) for both the EFs and the LDOS. It should also be noticed that the maximum N extends over a greater energy range for even Ce and odd Pr, in both coupling conditions and for both EFs and LDOS, than those of odd Ce and even Pr. The maxima N occur in the lower-energy region for even Ce and odd Pr, whereas they occur in the higher-energy region for odd Ce and even Pr. Note that the N for the corresponding LDOS and EFs for each parity and coupling are very similar in shape and magnitude.

The N for the Lorentzian, squared Lorentzian and interpolated exponential fit are very close in value; however, the Gaussian fitted N show a substantial disagreement. This may be simply due to the form of the Gaussian function used. Note that the N for odd Ce is ≈ 50 less than that calculated in [1]; however, the N for even Ce shows agreement with that found in [1]. The spreading width Γ for the EFs indicates the energy region over which substantial mixing between basis states occurs around the unperturbed centroid basis state. Γ for the LDOS indicates the width of the energy region over which the initial unperturbed basis state

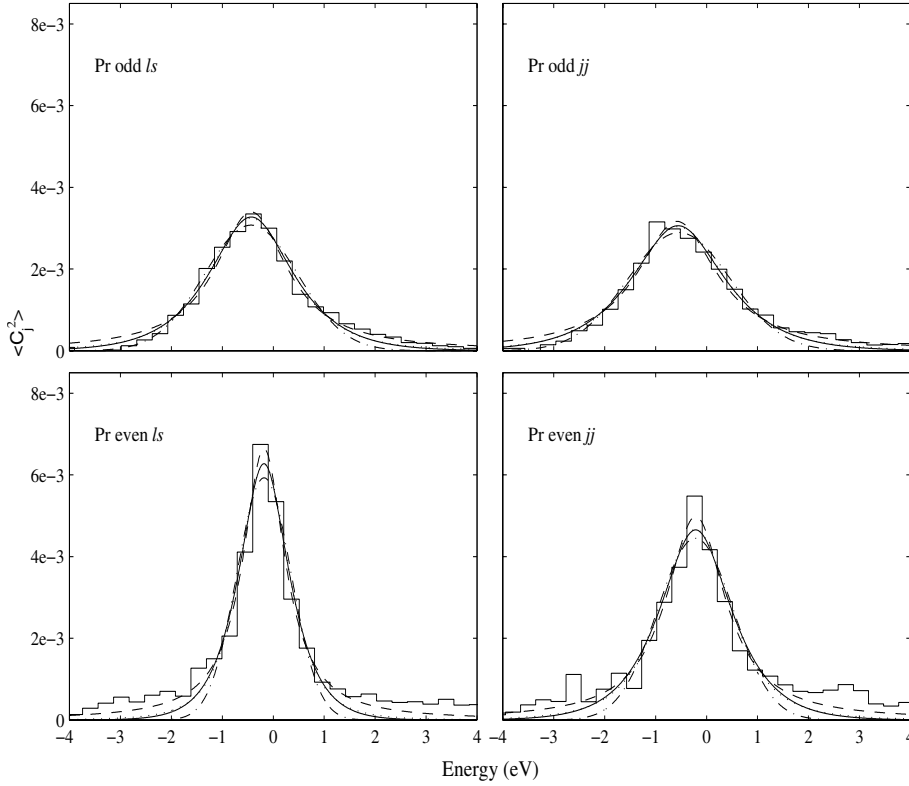


Figure 23. Selected window-averaged LDOS for Pr and least-squares fitting to (i) Lorentzian (dashed), (ii) squared Lorentzian (dotted), (iii) interpolation exponential (solid) and (iv) Gaussian (dash-dot).

becomes ‘spread’. Γ was found to be fairly constant at 0.5–1.5 eV for Ce and Pr in both the EFs and LDOS and for both coupling conditions. Similar Γ s for the EFs and the LDOS for both Ce and Pr indicate that the two-body interaction in the Hamiltonian is relatively small. Also, the LDOS tended to have a greater width than that of the EFs by sometimes a value of 1–1.5 eV, although this depends on the energy region considered. Note that the Γ s for the EFs are approximately two to three times smaller than that calculated in [1] for Ce, the coupling schemes used being the determining factor. Fermi’s golden rule gives for the BW function

$$\Gamma_{\text{BW}} = 2\pi \frac{\overline{V^2}}{D} \quad (16)$$

where $V = \langle a | \underline{H} | b \rangle$, $a \neq b$ (i.e. off-diagonal elements) and $\overline{\quad}$ indicates the mean.

Using the H_{ij}^2 values of tables 2–5 (the whole matrix values) the Γ_{BW} were calculated and are tabulated in table 8.

From table 8 it can be seen that Ce has values of $\Gamma_{\text{BW}} \approx 0.6$ – 0.7 eV, whereas Pr has values of ≈ 0.8 – 1.0 eV. There is also no substantial difference between the Γ_{BW} s of the corresponding coupling schemes. These values are consistent with the Γ s calculated via the Lorentzian and interpolation exponential curve fits.

The energy shifts ΔE were found to be very similar for all of the distributions and vary from -0.5 to 1.0 eV for the EFs of Ce and from -1.0 to 3 eV for the LDOS of Ce. ΔE for

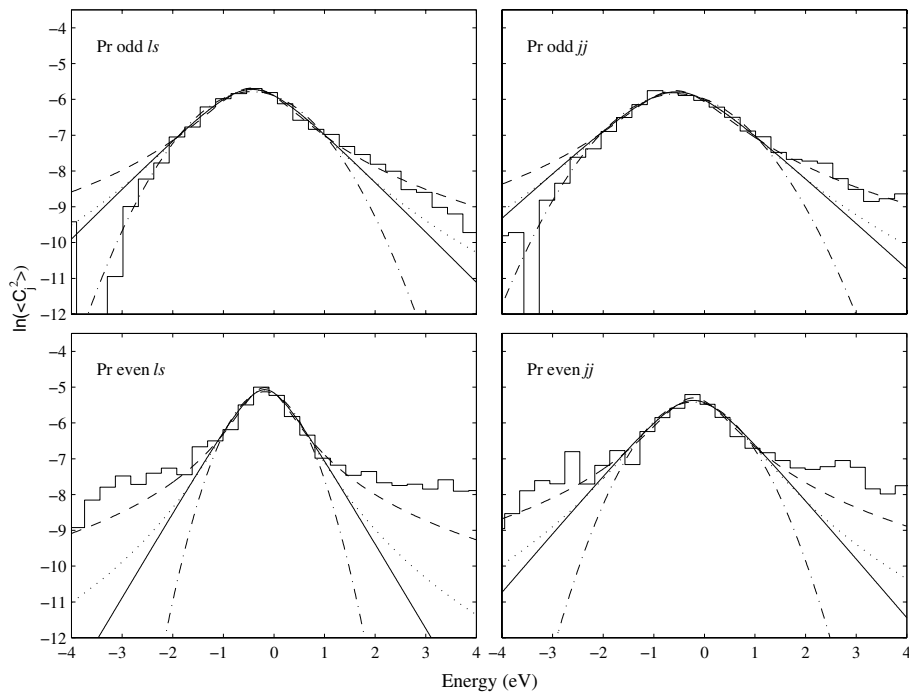


Figure 24. Selected window-averaged LDOS for Pr with a semi-logarithmic scale.

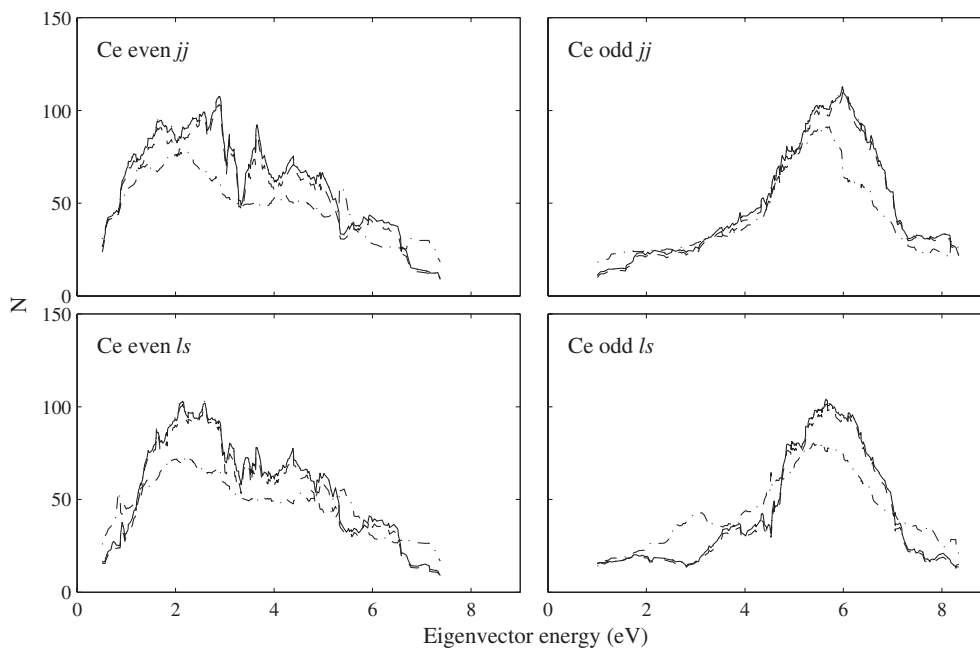


Figure 25. The number of principal components N for the EFs of Ce.

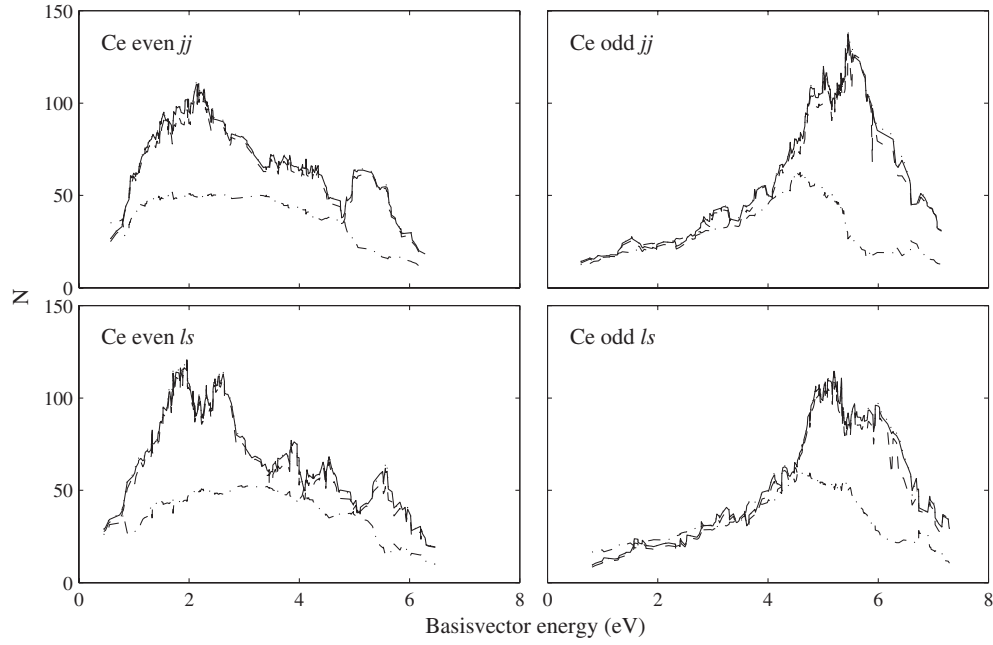


Figure 26. The number of principal components N for the LDOS of Ce.

Table 8. Γ_{BW} for even and odd Ce and Pr, calculated via Fermi's golden rule.

	Ce				Pr			
	Even		Odd		Even		Odd	
	<i>ls</i>	<i>jj</i>	<i>ls</i>	<i>jj</i>	<i>ls</i>	<i>jj</i>	<i>ls</i>	<i>jj</i>
$\Gamma_{\text{BW}} = 2\pi \frac{\overline{H_{ij}^2}}{D}$ (eV)	0.65	0.72	0.61	0.68	0.94	1.02	0.77	0.82

the EFs of Pr range from -0.25 to 1.5 eV and -1.0 to 4.0 eV for the LDOS of Pr. Note that there was 'divergence' of ΔE in the higher-energy regions, which indicates the presence of 'shoulders' that overweight the calculated position of the centroid energy.

In [12] it also states that the correspondence between the shapes of the LDOS and EFs is still open; however, from the studies up to now, one can conclude that if the width of the perturbed spectrum is of the same order as the unperturbed one, one can expect that both shapes are very close to each other.

5. Density of states

The validity of the Lorentzian, squared Lorentzian and interpolation exponential distributions is checked by using the normalization condition of equation (4.12) of [1]:

$$\frac{\Gamma}{ND} \int_{-\infty}^{+\infty} f(\varepsilon) d\varepsilon = 1 \quad (17)$$

where D is the local average level spacing. For the Lorentzian and squared Lorentzian $\int_{-\infty}^{+\infty} f(\varepsilon) d\varepsilon = \frac{\pi}{2}$ and $\frac{\pi}{4}$ respectively. In this paper $\int_{-\infty}^{+\infty} f(\varepsilon) d\varepsilon$ was found to be, numerically,

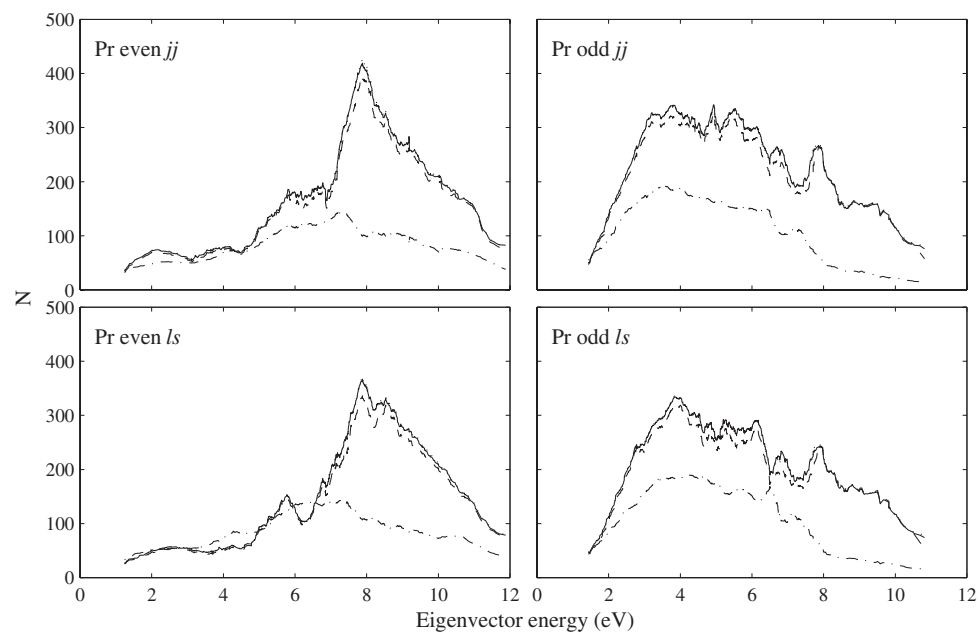


Figure 27. The number of principal components N for the EFs of Pr.

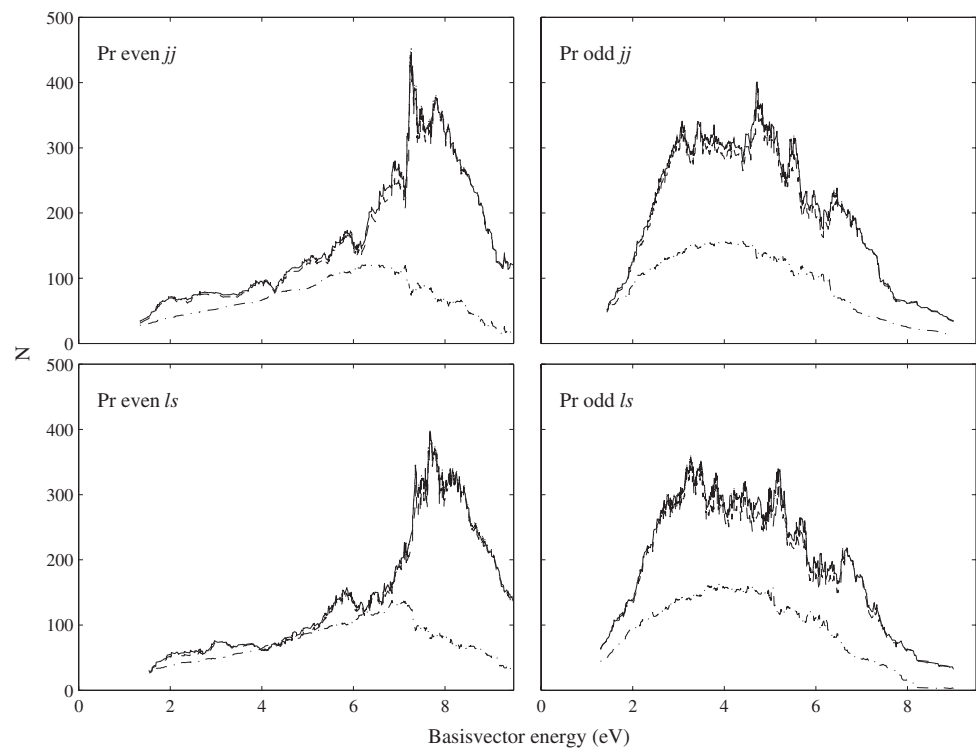
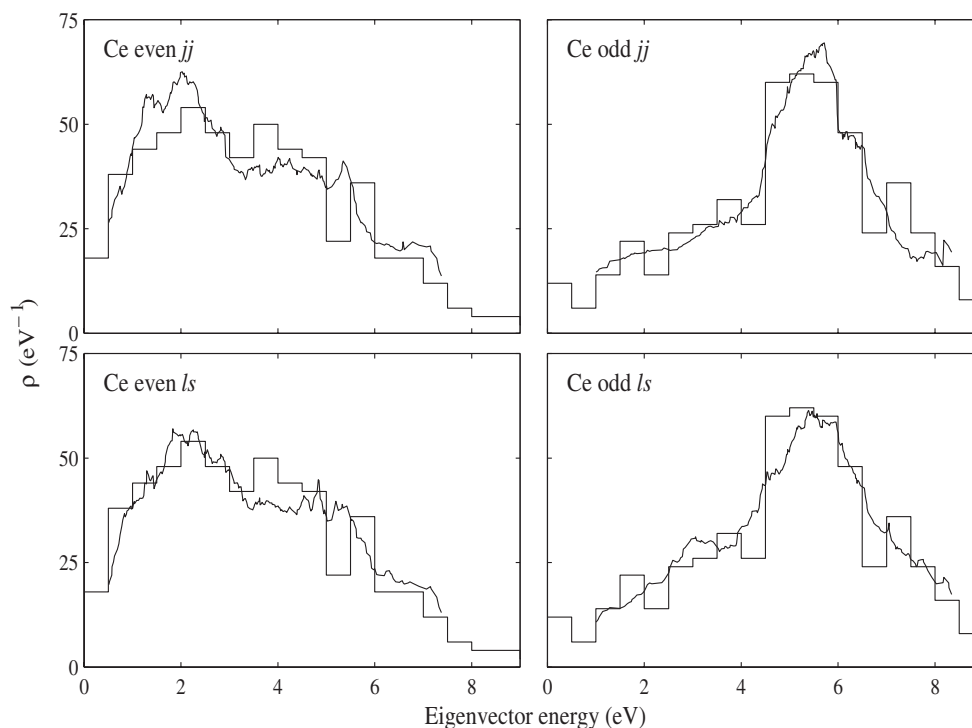


Figure 28. The number of principal components N for the LDOS of Pr.

Table 9. Density of states, $\rho(E)$, for the Lorentzian, squared Lorentzian and interpolation exponential distributions.

$\rho(E) = \frac{2N}{\pi\Gamma}$	Lorentzian
$\rho(E) = \frac{4N}{\pi\Gamma}$	Squared Lorentzian
$\rho(E) = \frac{N}{1.636\Gamma}$	Interpolation exponential

**Figure 29.** The density of states of Ce shown by the histogram and the density of states calculated using N and Γ from the Lorentzian curve fit.

approximately equal to 1.636 for the interpolation exponential $f(\varepsilon)$. Table 9 summarizes the various densities of states $\rho(E)$ corresponding to different distributions.

Figures 29 and 30 compare the calculated density of states ρ for Ce and Pr with the value of ρ of the Lorentzian distribution. It was found that the ρ given by the Lorentzian distribution appears to be the better approximation for the density of states.

The corresponding unperturbed densities of states are shown in figures 31 and 32. The effect of non-configuration interaction is clearly visible in the histograms with the appearance of very large ‘fluctuations’ compared with that seen in the configuration interaction histograms. Thus the $\rho(E)$ given in table 9 are ‘too smooth’ for the unperturbed density of states.

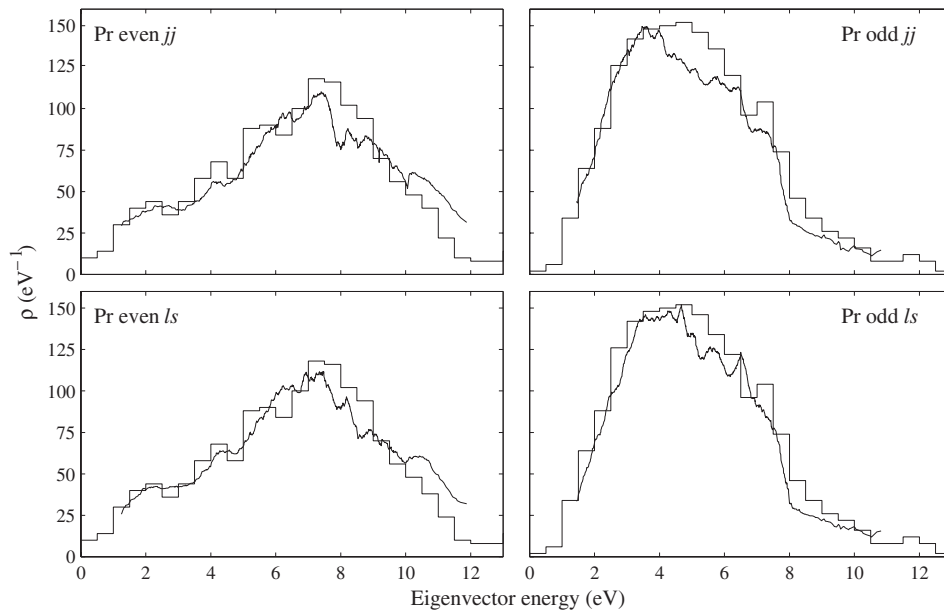


Figure 30. The density of states of Pr shown by the histogram and the density of states calculated using N and Γ from the Lorentzian curve fit.

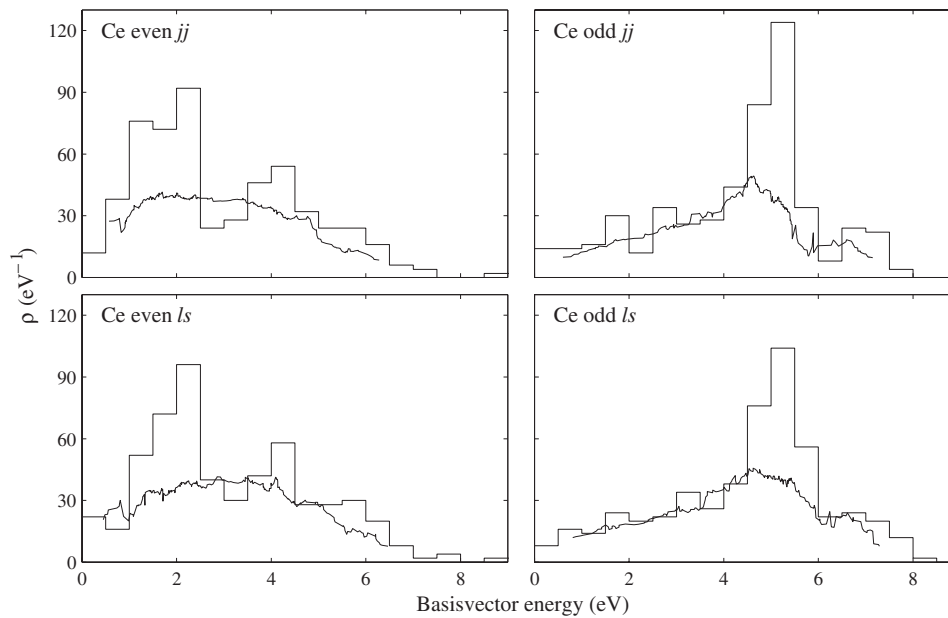


Figure 31. The unperturbed density of states of Ce shown by the histogram and the density of states calculated using N and Γ from the Lorentzian curve fit.

6. The statistics of C_{ij}

In [1] it was concluded that the C_{ij} of Ce calculated using an HFD calculation have statistics close to that of independent random variables and they tend towards Gaussian (and hence to a

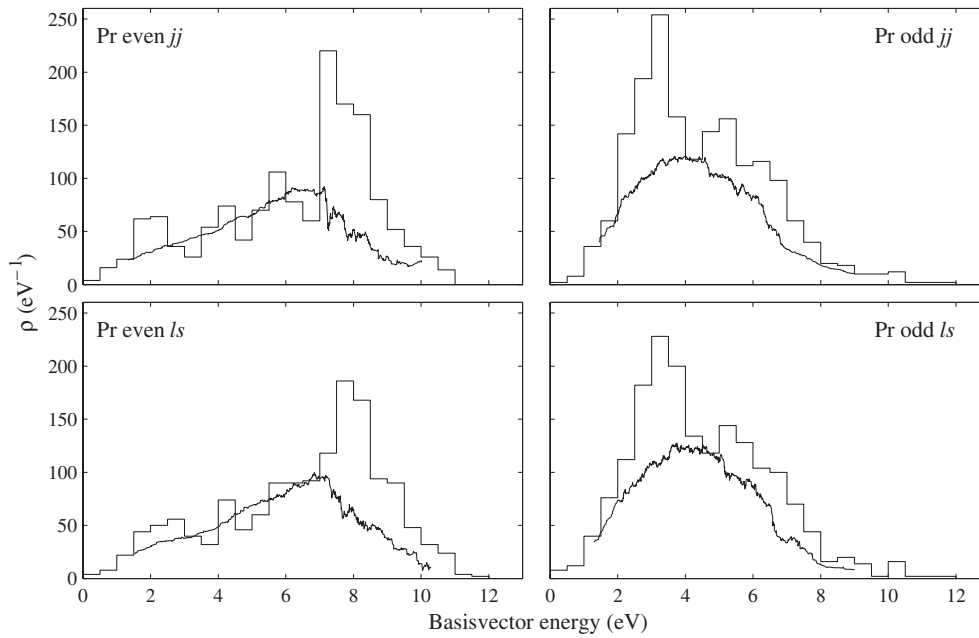


Figure 32. The unperturbed density of states of Pr shown by the histogram and the density of states calculated using N and Γ from the Lorentzian curve fit.

Porter–Thomas distribution for $|C_{ij}|^2$) when the configuration interaction (mixing) is strong. To test this conclusion the normalized window-averaged EFs were evaluated for Ce and Pr (the $C_{ij}/\sqrt{\langle C_{ij}^2 \rangle}$ were evaluated). The SSRs for curve fitting to the previously given $f(\varepsilon)$ distributions for Ce and Pr are shown in figure 33. The curve fitting was between ≈ -3.5 and 3.5 eV. The 75th state and the 150th state are shown for even Ce and odd Ce respectively, while the 232nd and 332nd states are shown for odd and even Pr respectively, in figures 34–37.

It can be seen that the smallest SSR occurs for the interpolation exponential, for both Ce and Pr, the exception being the odd Pr in jj coupling, where the Gaussian $f(\varepsilon)$ has the smallest SSR. Note that the squared Lorentzian SSRs are in fact very similar in value to the corresponding interpolation exponential SSRs. It can also be seen that the largest SSRs occur in general for the Lorentzian curve ‘fits’. Looking at figures 34 and 36, it is quite difficult to distinguish any substantial differences in the curve fittings, apart from in the tails of the functions. The deviations from the distribution tails can be seen in figures 35 and 37 with their semi-logarithmic scales. For odd and even Ce in ls coupling there is good agreement with the interpolation exponential $f(\varepsilon)$. The tails, however, drop faster than exponentially in the jj coupling of even and odd Ce. Thus the tails of the C_{ij} distributions appear to differ in the two coupling schemes considered. Whether this is significant or not is highly dependent on the curve fitting procedure and the range over which the curve fitting is determined. This aspect needs further investigation.

The tails of the Pr distributions consistently appear to ‘fall’ more quickly than exponentially. However, the fits may be closer to exponential if curve fitting only to the tails was used.

From the present results it would appear that only for the odd Pr C_{ij} , in jj coupling, is there the possibility of Gaussian and hence ‘chaotic’ eigenvector components. However,

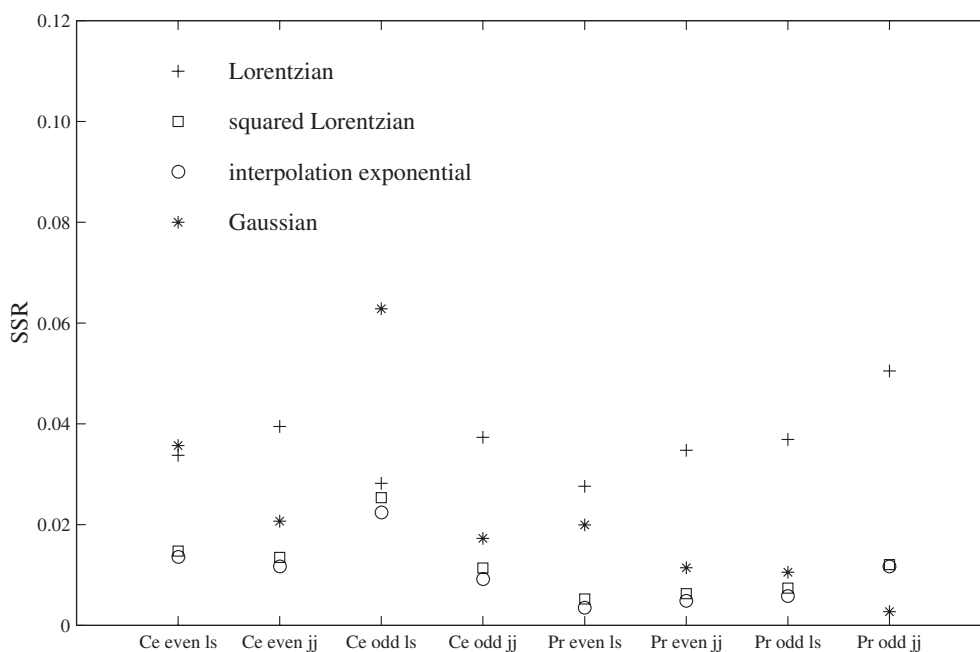


Figure 33. Sum of the square of the residuals (SSR) for least-squares fitting to (i) Lorentzian, (ii) squared Lorentzian, (iii) interpolation exponential and (iv) Gaussian for various normalized EFs of Ce and Pr.

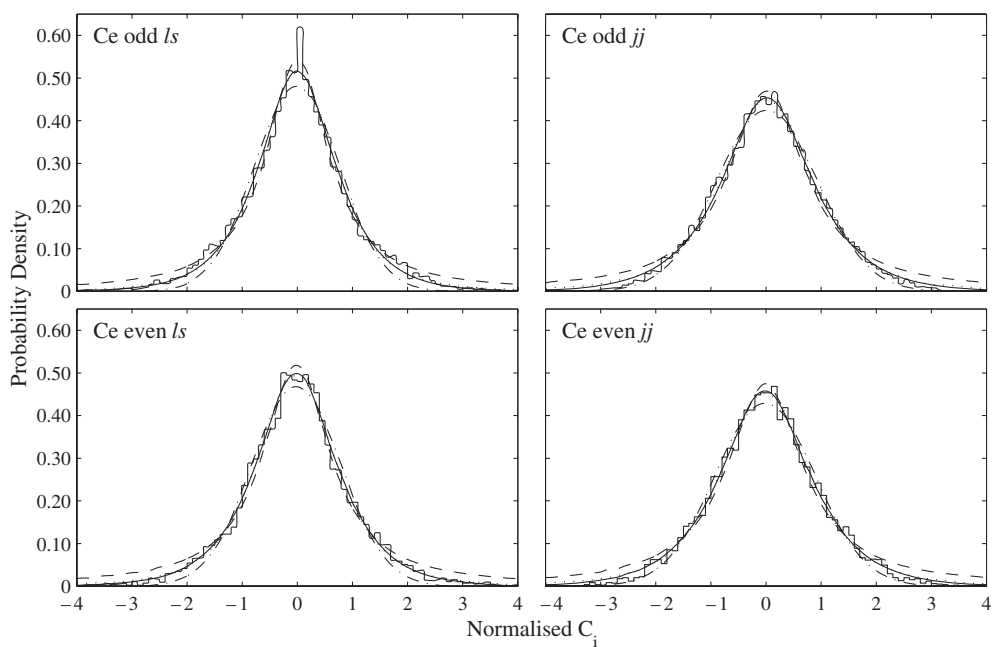


Figure 34. Selected window-averaged normalized EFs for Ce and least-squares fitting to (i) Lorentzian (dashed), (ii) squared Lorentzian (dotted), (iii) interpolation exponential (solid) and (iv) Gaussian (dash-dot).

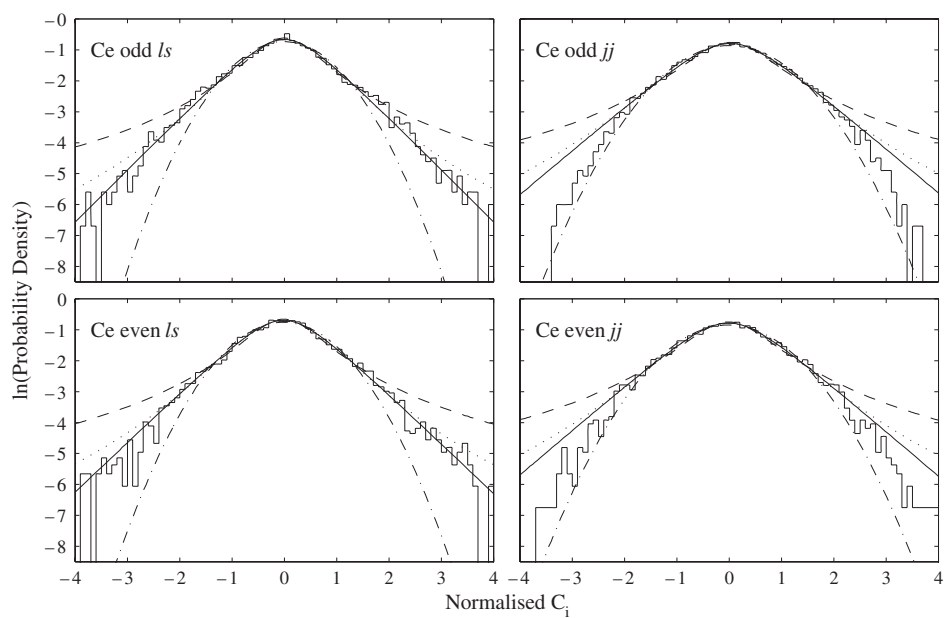


Figure 35. Selected window-averaged normalized EFs for Ce with a semi-logarithmic scale.

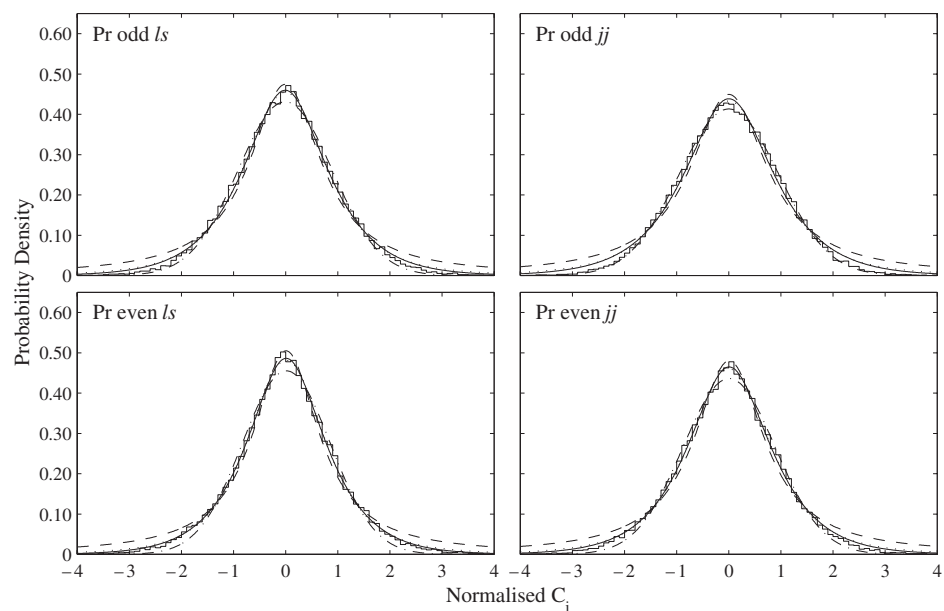


Figure 36. Selected window-averaged normalized EFs for Pr and least-squares fitting to (i) Lorentzian (dashed), (ii) squared Lorentzian (dotted), (iii) interpolation exponential (solid) and (iv) Gaussian (dash-dot).

the presence of basis representation dependence and the combinatorial nature of basis state coupling, particularly at a high level density, must be taken into consideration when claiming apparent random and Gaussian statistics.

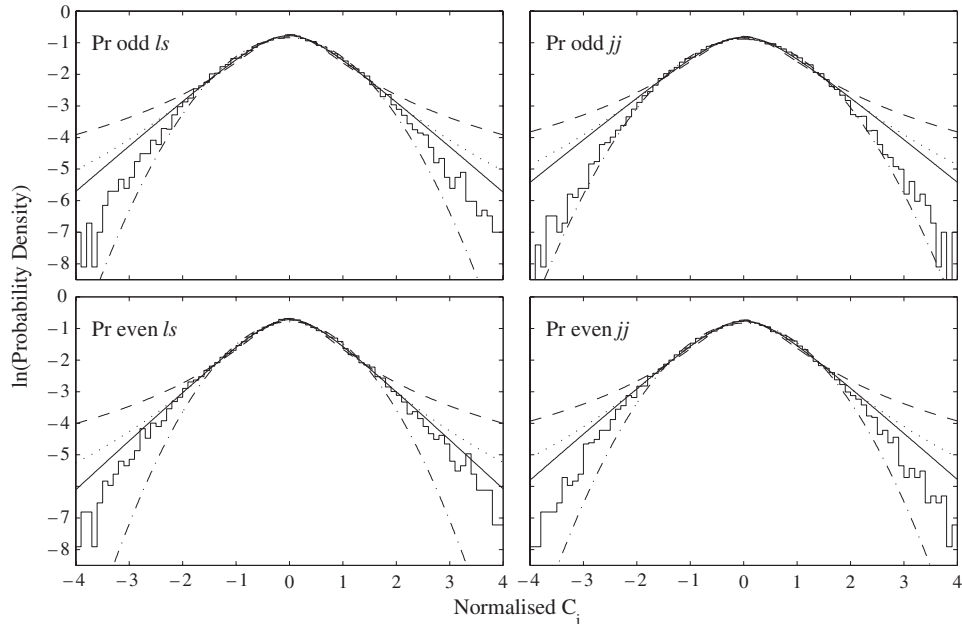


Figure 37. Selected window-averaged normalized EFs for Pr with a semi-logarithmic scale.

7. The tails of the LDOS and EFs

Plotting the logarithms of the LDOS and EFs as shown in figures 22 and 24 allows one to see that the calculated LDOS and EFs can, but do not always, ‘drop’ faster than the BW form and even as quickly or apparently quicker than exponentially. A modified exponential decay was predicted in [13, 14] beyond the energy bandwidth Db (D is the mean level spacing of the *unperturbed* energy levels) of the BRM model

$$w(E_i; E, \Gamma, N) \propto \exp \left[-2\xi \ln \left(\xi e^{-1} \sqrt{2q^{-1} \ln [\xi/\sqrt{q}]} \right) \right] \quad (18)$$

where $\xi = \frac{|E-E_i|}{Db}$, $q = \frac{V^2}{D^2b}$ and where $w(E_i; E, \Gamma, N)$ has been corrected in [1].

In [16] it was found, from a direct comparison of the LDOS and EFs, that there was ‘localization in the energy shell’ for conservative systems with chaotic behaviour—this is a semi-classical result.

8. Complexity of wavefunction components

The information entropy, S [17–20], is an appropriate statistic for measuring the degree of complexity of individual wavefunction components C_{ij} . It can be defined for a given normalized wavefunction $|j\rangle$ and expanded with the aid of a given basis $|i\rangle$, in terms of the weights of the components

$$S^j = -\sum_i W_i^j \ln(W_i^j) \quad (19)$$

where $W_i^j = (C_i^j)^2$ and $C_i^j =$ normalized amplitude. When the amplitudes C_i^j are normally distributed with $\bar{C} = 0$ and $\overline{C^2} = 1/N$ the exact GOE distribution reduces to a Gaussian distribution [4]:

$$P(C) = (N/2\pi)^{1/2} \exp\left(-\frac{N}{2}C^2\right). \quad (20)$$

The weights $W = C^2$ of the components thus obey the Porter–Thomas distribution

$$P(W) = (N/2\pi)^{1/2} \frac{1}{\sqrt{W}} \exp\left(-\frac{N}{2}W\right). \quad (21)$$

The same amplitudes C_i^j describe the fragmentation of a simple state $|i\rangle$ over exact eigenstates $|j\rangle$.

In a given energy range, $E \approx E_j$, the distribution of components C_i^j is similar to the Gaussian one but with the local width $(C_i^j)^2 = 1/N_j$:

$$P^j(C^j) = \left(\frac{N_j}{2\pi}\right)^{1/2} \exp\left(-\frac{N_j}{2}(C^j)^2\right) \quad (22)$$

where N_j is the the number of principal components [4].

The entropy S^j , or the corresponding length in Hilbert space $l_s^j = \exp(S^j)$, characterizes the degree of delocalization of a given eigenfunction $|j\rangle$ with respect to an original basis. The deviation of l_s^j from the GOE limit $0.482N$ indicates the incomplete mixing of basis states [4].

For a similar purpose one can use [19] the moments of the distribution of amplitudes

$$M_n^j = \sum_i (W_i^j)^n \quad (23)$$

which are also related to the effective number of principal components (NPC) of a given eigenstate (see later).

Figures 38 and 39 show the calculated $\exp(S^\alpha)$, the information length, where α represents either the eigenvectors $|j\rangle$ or the basis vectors $|i\rangle$. It can be observed that in the most ‘chaotic’ part of the spectrum the information entropy does not reach the GOE value, $N_j = N$, which would give $S^\alpha = \ln(0.482N)$ ($\Rightarrow l_s^\alpha = 0.482N$). The entropy of the most ‘chaotic’ states is approximately 55%, i.e. roughly half, of that expected for the GOE. This is the case for all of the parities and couplings for both Ce and Pr. As was stated earlier this indicates incomplete mixing of the basis states. Note the fluctuations, which indicate that neighbouring states are different.

A typical pattern of the ‘regular’ bell-shape behaviour of information entropy S is formed due to the configuration interaction and is more visible for Pr. This Gaussian shape appears to be generic [4]. In [4] it was found that the degree of localization of EFs depends strongly on the strength of the configuration interaction. Thus it was found that the general trend of the mean field was to quench the chaotic signatures of many body dynamics [4].

Other possible measures of complexity are [4] the following:

- (i) The effective NPC is defined from the participation index

$$(\text{NPC})^j = (M_2^j)^{-1} \quad (24)$$

i.e. the NPC of the j th eigenstate.

- (ii) For a Gaussian distribution of components C_i^j

$$\frac{l_s^j}{(\text{NPC})^j} = 1.44. \quad (25)$$

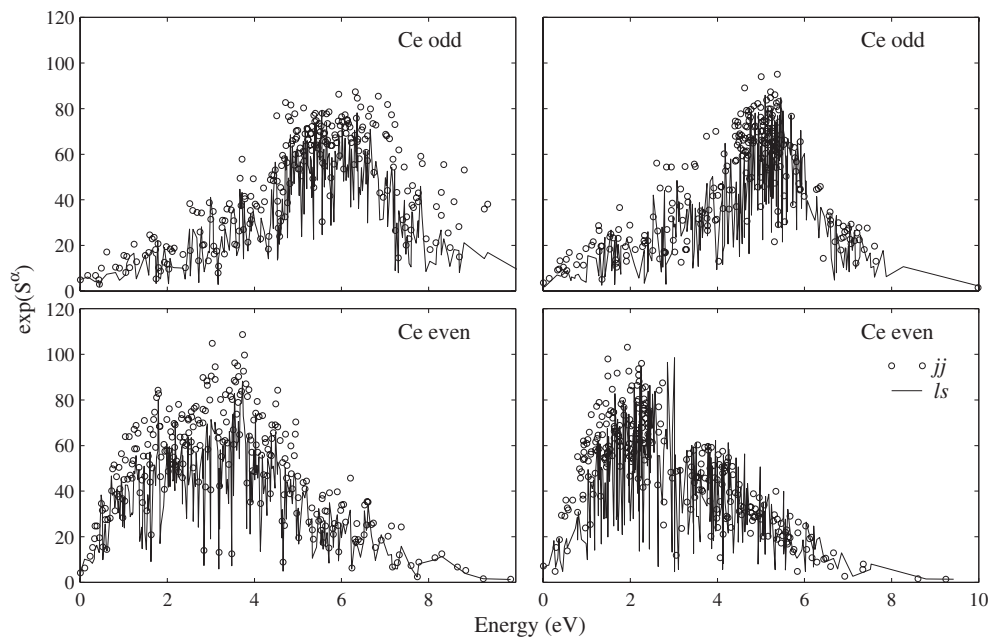


Figure 38. The information length $\exp(S^\alpha)$ for Ce in ls and jj coupling. The left-hand column corresponds to the $\exp(S^\alpha)$ of the eigenvectors, whereas the right-hand column is $\exp(S^\alpha)$ of the basis vectors.

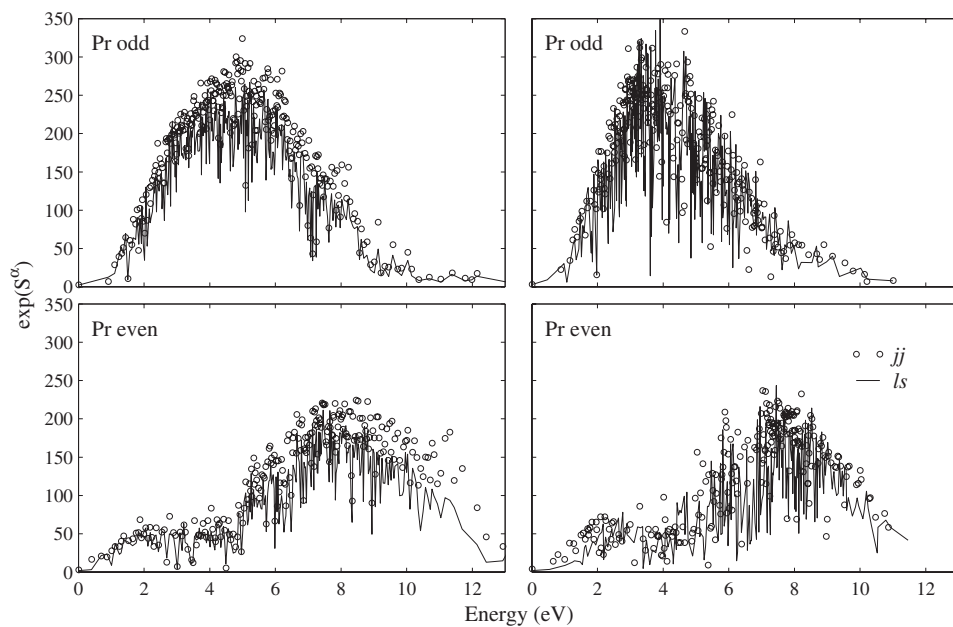


Figure 39. $\exp(S^\alpha)$ for Pr in ls and jj coupling.

Figures 40 and 41 show the NPC for the eigenvectors and basis vectors of Ce and Pr. It can be seen that the NPCs are roughly 50–55% of the GOE value of $N/3$ at the maxima of the NPC.

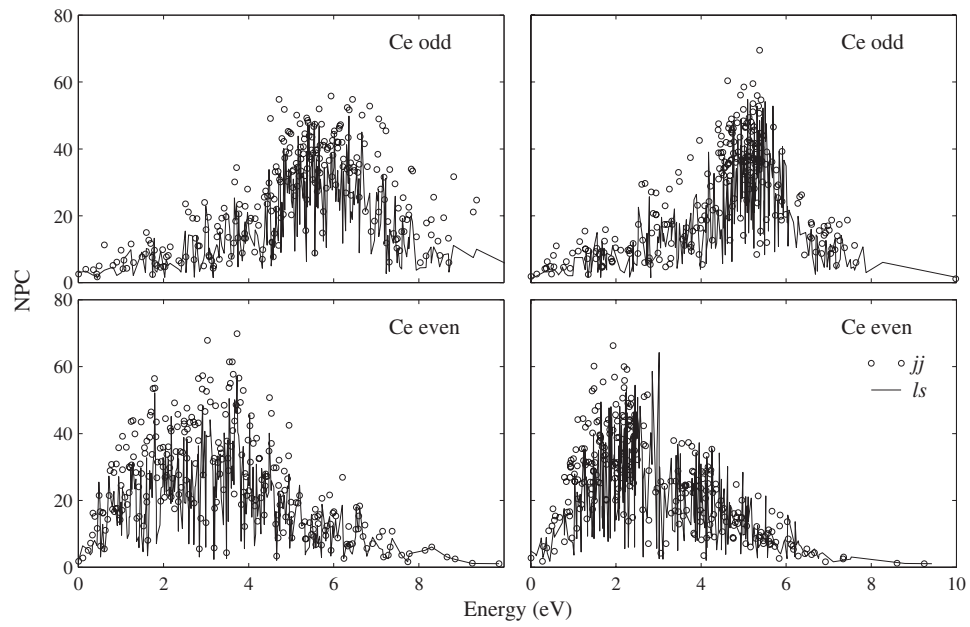


Figure 40. NPC for Ce in ls and jj coupling. The left-hand column corresponds to the eigenvectors, whereas the right-hand column corresponds to the basis vectors.

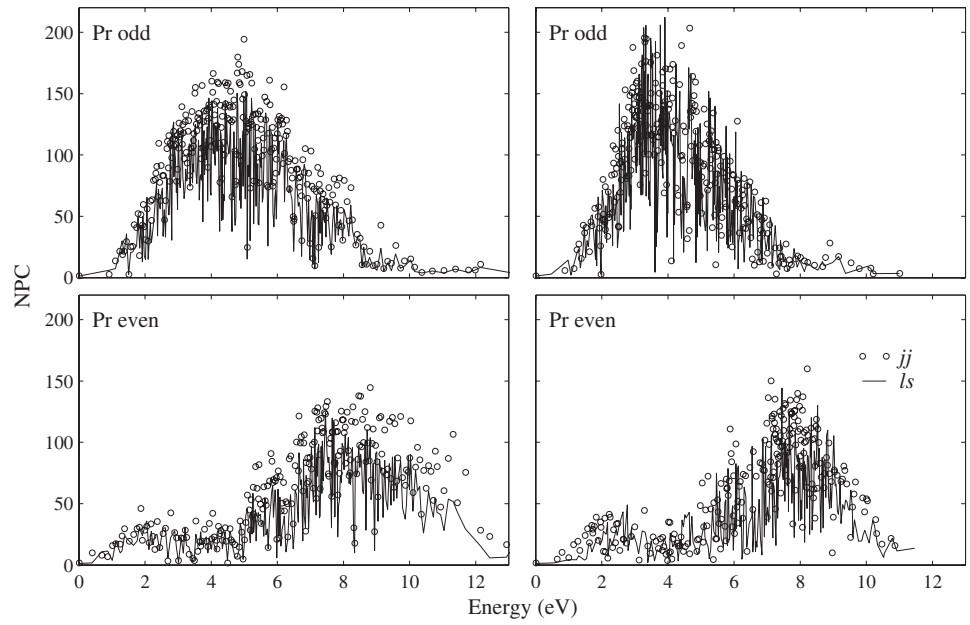


Figure 41. NPC for Pr in ls and jj coupling.

This indicates a finite localization length. Note that the maxima of the effective NPC are very roughly one-half of the maxima of the NPC as calculated by the curve fitting of section 4.

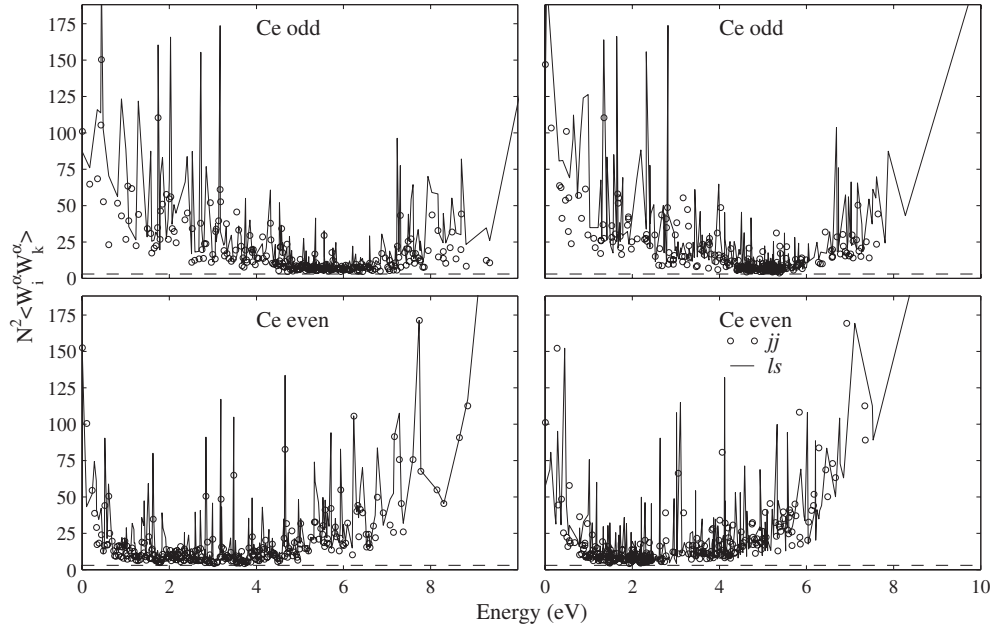


Figure 42. $N^2 \langle W_i^\alpha W_k^\alpha \rangle$ for Ce for $k = i$. The left-hand column corresponds to the eigenvectors whereas the right-hand column corresponds to the basis vectors.

9. Correlations of eigenvector components

In the limit $N \gg 1$ the correlation function of the weights is [4]

$$N^2 \langle W_i^\alpha W_k^\beta \rangle = (1 + 2\delta_{\alpha\beta}\delta_{ik}). \quad (26)$$

The correlation function of (26) is shown in figures 42–45 for Ce and Pr. Note that α represents the eigenvectors or the basis vectors. The $N^2 \langle W_i^\alpha W_k^\beta \rangle$ are calculated by keeping α fixed in the product $W_i^\alpha W_k^\beta$, with $\beta = \alpha$, and averaging over all components i and k , keeping a constant value of the ‘distance’ $k - i$ (where $k \geq i$). The correlation function for the diagonal ($i = k$) has a GOE value of 3.0, corresponding to the random distribution of the orthogonal unit vectors over the surface of the $(N - 1)$ -dimensional sphere in N -dimensional space. However in figures 42 and 43 it can be seen that there is significant deviation from the GOE prediction, particularly at the edges of the spectra where there is smaller complexity and larger typical weights of the components of these states. As $k - i$ increases, $N^2 \langle W_i^\alpha W_k^\beta \rangle$ becomes closer to unity as given by the GOE prediction for $k \neq i$. However, even for $k - i = 30$ there is still deviation from the GOE limit, particularly at the edges of the spectrum, i.e. there is incomplete mixing of ‘basis’ states.

However, it should be noted that the essential shortcoming of using such characteristics as information entropy or the moments of the distribution function of the components is their inability to distinguish ‘genuine’ chaotic behaviour from the complexity associated with collective motion or with improper choice of the basis [4].

10. Localization length

The ‘size’ of the basis which eigenstates occupy is defined via the localization length. There are two localization lengths, namely, the ‘entropy localization length’ l_h and the ‘localization

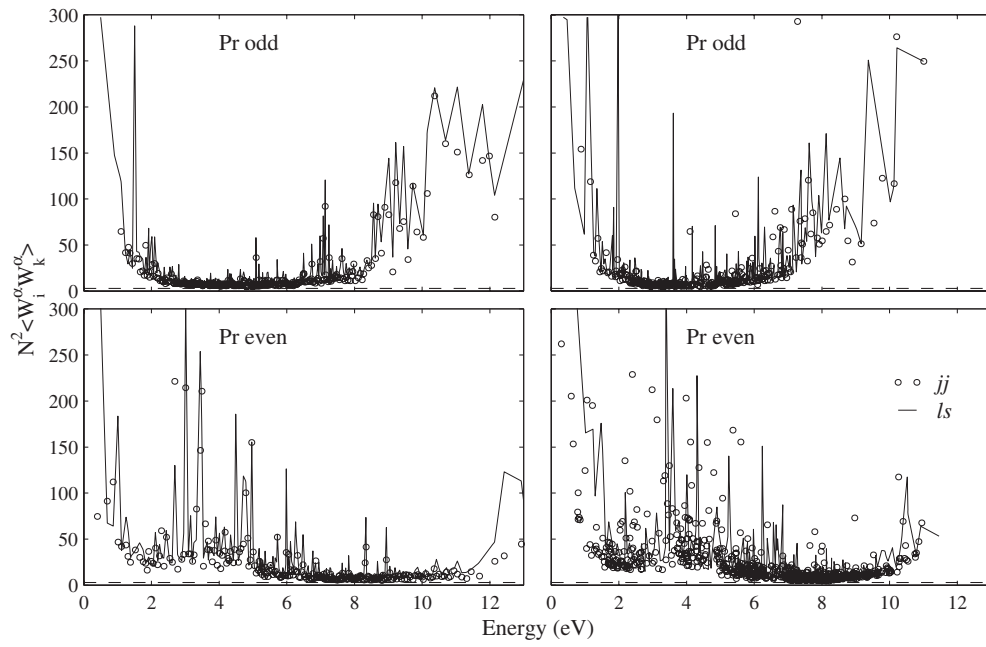


Figure 43. $N^2 \langle W_i^\alpha W_k^\beta \rangle$ for Pr for $k = i$

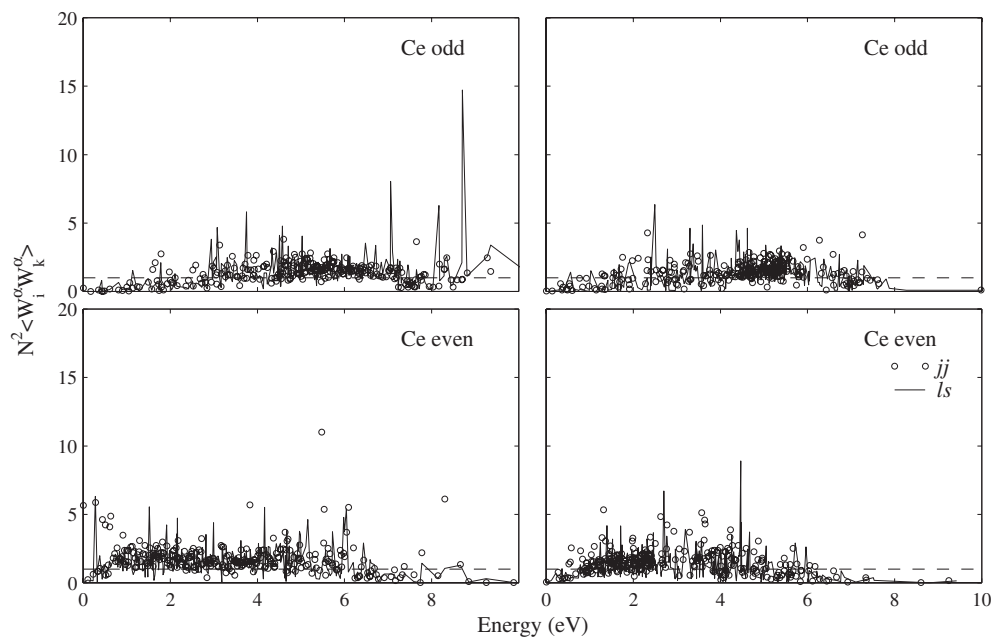


Figure 44. $N^2 \langle W_i^\alpha W_k^\beta \rangle$ for Ce for $k - i = 30$.

length' l_{ipr} associated with the participation ratio. The entropy localization is defined as

$$l_h = N \exp(\langle H \rangle - H_0) \quad (27)$$

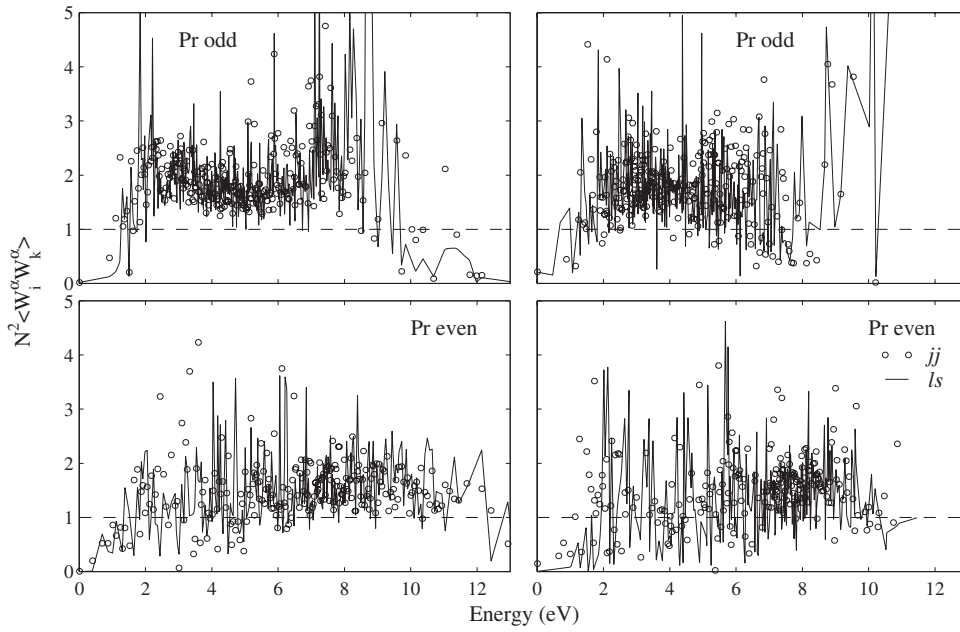


Figure 45. $N^2 \langle W_i^\alpha W_k^\beta \rangle$ for Pr for $k - i = 30$.

where $\langle H \rangle$ is the mean entropy of eigenstates

$$\langle H \rangle = -\frac{1}{M} \sum_{n=1}^M \sum_{i=1}^N W_i^n \ln(W_i^n) \quad (28)$$

and H_0 is the normalization constant, which is equal approximately to 2.078 in the pure Gaussian fluctuations of C_i [17]. Here M is the number of eigenstates which are taken for the average ($M = 1$ was used in this paper).

Assuming the Gaussian character of fluctuations of the components of eigenstates, the second definition of the localization length l_{pr} is given by

$$l_{\text{pr}} = \frac{3}{P} \quad \text{where} \quad P = \frac{1}{M} \sum_{n=1}^M \sum_{i=1}^N (W_i^n)^2. \quad (29)$$

In order to compare the characteristics of the eigenvectors and basis vectors, the dependence of the entropy localization length l_h on the energy is shown for both Ce and Pr in figures 46–49. Apart from strong fluctuations in general, the dependences $l_h(E)$ look very similar, i.e. increase to a maximum and then decrease. It can be seen that the l_h only reach approximately 55–60% of the GOE values of N (the matrix size) for both ls and jj coupling. Also, there is no significant difference between the l_h of the different coupling schemes. The circles in figures 46–49 indicate $4 \cdot \text{NPC}$, which is the prediction of [1] for l_h for the Lorentzian distribution. Note that, as in [1], the NPC as found by curve fitting gives $l_h \approx (1-2) \cdot \text{NPC}$. Whether this indicates deviation from Lorentzian behaviour is not fully understood.

11. Conclusion

It has been found that the distribution of the off-diagonal many-body matrix elements of the HFCI method and in both the ls and jj coupling schemes is close to exponential, which seems

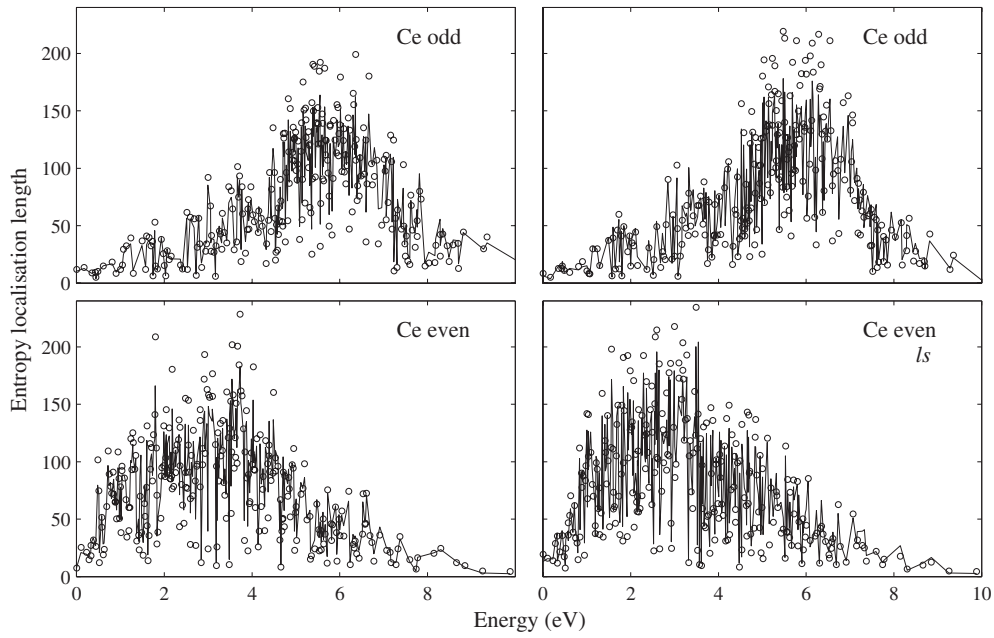


Figure 46. Entropy localization length for Ce in ls coupling. The left-hand column corresponds to the eigenvectors, whereas the right-hand column corresponds to the basis states. The solid line indicates l_n , whereas the circles correspond to 4-NPC.

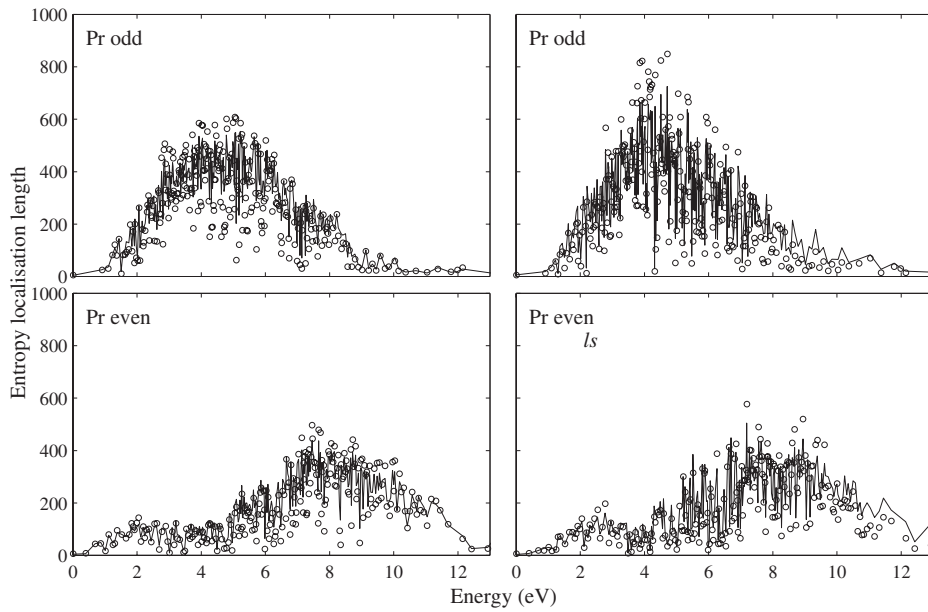


Figure 47. Entropy localization length for Pr in ls coupling.

to be a generic feature for realistic systems [1, 4]. The Hamiltonian does not contain any random elements and any possible ‘chaoticity’ arises as a result of mixing of the basis states.

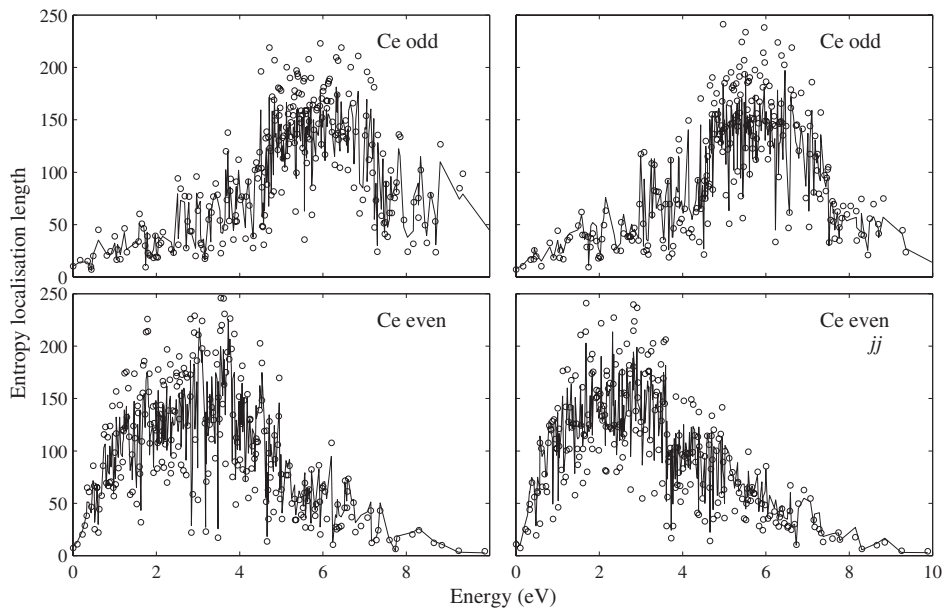


Figure 48. Entropy localization length for Ce in jj coupling.

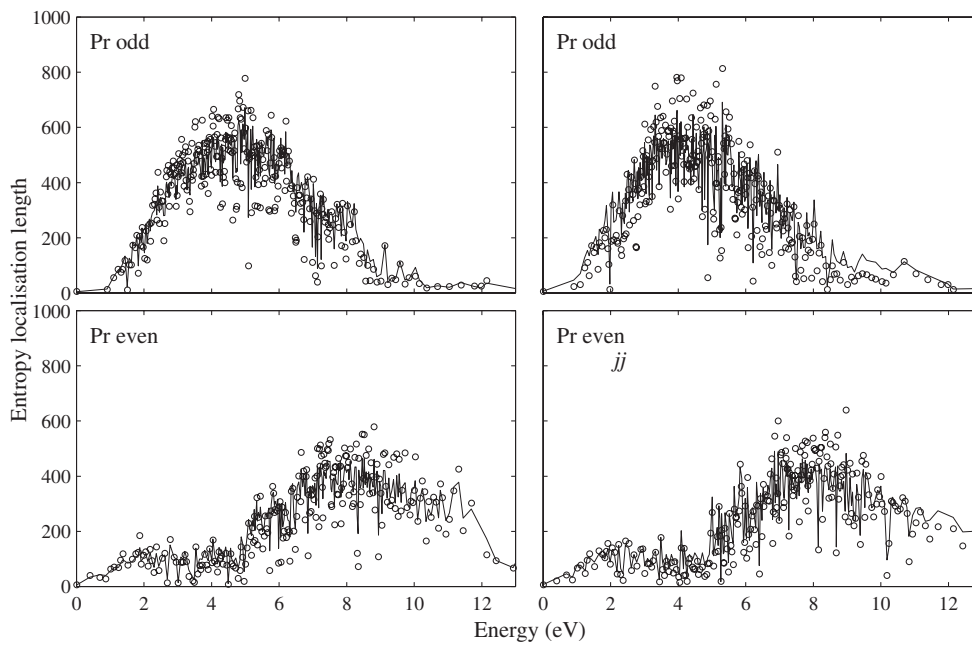


Figure 49. Entropy localization length for Pr in jj coupling.

In general the central maxima of the EFs and LDOS are Lorentzian in ‘shape’ whereas the tails deviate from the Lorentzian distribution. In fact the Lorentzian over-estimates the weight of the remote components. In [15] it states that the BW form for the strength function is an immediate consequence of the assumption of constant coupling between matrix elements.

The evolution of the shape of the EFs and the LDOS as a function of perturbation should be included in future studies, for example, the effect of changing the single configuration radial integrals, F^k and G^k , and the configuration interaction radial integrals, R^k .

The degree of complexity of wavefunctions can be measured by the information entropy and the moments of the distribution function of the wavefunction components C_{ij} . However, these measures depend on the basis representation that is used.

Acknowledgments

This paper was supported by the Irish science and technology agency Enterprise Ireland under research grant no SC-99-206. We would like to thank one of the referees for their helpful comments.

References

- [1] Flambaum V V, Gribakina A A, Gribakin G F and Kozlov M G 1994 *Phys. Rev. A* **50** 267–96
- [2] Gribakina A A, Flambaum V V and Gribakin G F 1995 *Phys. Rev. E* **52** 5667
- [3] Flambaum V V, Gribakina A A and Gribakin G F 1998 *Phys. Rev. A* **58** 230–7
- [4] Zelevinsky V, Brown B A, Frazier N and Horoi M 1996 *Phys. Rep.* **276**
- [5] Fyodorov Y V, Chubykalo O, Izrailev F M and Casati G 1996 *Phys. Rev. Lett.* **76** 1603
Wang W, Izrailev F M and Casati G 1998 *Phys. Rev. E* **57** 323–39
- [6] Mehta M L 1991 *Random Matrices* 2nd edn (New York: Academic)
- [7] Cowan R D 1981 *The Theory of Atomic Structure and Spectra* (Berkeley, CA: University of California Press)
- [8] http://physics.nist.gov/cgi-bin/AtData/main_asd
- [9] Casati G, Molinari L and Izrailev F 1990 *Phys. Rev. Lett.* **64** 1851–4
- [10] Kús M, Lewenstein M and Haake F 1991 *Phys. Rev. A* **44** 2800
- [11] Fyodorov Y V and Mirlin A D 1991 *Phys. Rev. Lett.* **67** 2405
Fyodorov Y V and Mirlin A D 1994 *Int. J. Mod. Phys. B* **8** 3795
- [12] Izrailev F M 1999 Quantum chaos and thermalization for interacting particles *Proc. Int. School of Physics 'Enrico Fermi' (Varenna)*
- [13] Wigner E P 1955 *Ann. Math.* **62** 548
- [14] Wigner E P 1957 *Ann. Math.* **65** 203
- [15] Bohr A and Mottelson B R 1969 *Nuclear Structure* vol 1 (New York: Benjamin)
- [16] Casati G, Chirikov B V, Guarneri I and Izrailev F M 1996 *Phys. Lett. A* **223** 430
- [17] Izrailev F M 1990 *Phys. Rep.* **196** 299–392
- [18] Yonegawa F J 1980 *J. Non-Cryst. Solids* **35&36** 29
- [19] Reichl J 1988 *Europhys. Lett.* **6** 669
- [20] Zelevinsky V G 1993 *Nucl. Phys. A* **555** 109